これは，対象としている結節が充実型のみであるため，結節の境界は比較的明瞭であり，このような単純な処理でも抽出できているためである．しかし，今後はより多くの症例に適用できるよう，さらに精度の高いセグメンテーション手法を取り入れる必要がある．

5. むすび

本論文では，胸部 X 線 CT 像における小結節の良悪性鑑別のための画像特徴の定量化とそれに基づく分類の試みについて述べた．ある種の良性の結節（炎症性小結節）には頻繁に観察される画像所見があり，それらを結節の直径，結節と胸壁との距離，結節の境界における直線状部分の割合，結節の辺縁形状の複雑さ，結節内部の CT 値のばらつき，胸壁との間の細線の可視性の合計 6 つの特徴量として定量化した．得られた特徴量ベクトルから，その結節が炎症性小結節であるか否かを判別するために，ロジスティック回帰分析を用い，炎症性小結節 44 個とその他の結節 39 個に適用した．L 法による判別実験を行ったところ，正診率は 0.80 であった．各特徴量の有意性の仮説検定により，結節の直径，および結節内部の CT 値のばらつきに対して，有意水準 0.05 で有意性が認められた．

炎症性小結節ではないにもかかわらず医師が指摘する画像特徴を有する結節や，非常に小さく結節自体の特徴量を適切に計算できないものが存在した．このような結節の存在が判別を困難にしている．そのため，結節の周辺構造を定量的に表現する特徴量の開発が必要である．また，本稿で提案した特徴量の計算方法の改善，炎症性小結節と診断される結節に多く見られる画像特徴の組み合わせの考慮などを行うことで，さらなる精度改善を試みることが必要である．

謝　辞

日頃より熱心に御討論いただく名古屋大学村瀬研究室の諸氏に感謝する．本研究の一部は，文部科学省 21 世紀 COE プログラム：「社会情報基盤のための音声・映像の知的統合」，文部科学省・日本学術振興会科学研究費補助金，厚生労働省がん研究助成金，ならびに文部科学省私学 HRC 補助金による．

文　献

〔1〕 市川稚子，河田佳樹，仁木　登，他：良悪性鑑別における肺がん候補陰影の専門医判定結果の解析．信学技報 **MI2001-76**: 105-110, 2002

〔2〕 平野　靖，長谷川純一，鳥脇純一郎，他：胸部 CT 像からの 3 次元拡張ボロノイ分割による肺葉収縮の定量化．第 11 回コンピュータ支援画像診断学会大会・第 10 回日本コンピュータ外科学会大会合同論文集，2001, pp157-158

〔3〕 河田佳樹，仁木　登，大松広伸：胸部 3 次元 CT 像による肺野小型腫瘤の 3 次元曲率を用いた内部構造の解析．信学論 D-II **J83-D-II**(1): 209-218, 2000

〔4〕 平野　靖，目加田慶人，長谷川純一，他：胸部 X 線 CT 像における血管・気管支集束の 3 次元集中度を用いた定量化．Med Imag Tech **15**(3): 228-236, 1997

〔5〕 近藤真樹，平野　靖，長谷川純一，他：3 次元胸部 X 線 CT 像による腫瘤影の含気型と充実型への分類およびその良悪性鑑別への応用．信学技報（MI）**MI2000-16**: 27-32, 2000

〔6〕 金　亨燮，前門雅岐，石川聖二，他：肺 CT 像からのスリガラス状陰影候補領域抽出に関する一手法．第 22 回医用画像工学会大会講演論文集 PP-14, 2003

〔7〕 深野元太郎，中村嘉彦，滝沢穂高，他：Eigen Nodul：部分空間法を用いた胸部 X 線 CT 画像からの肺結節認識．第 22 回医用画像工学会大会講演論文集 OP4-15, 2003

〔8〕 Shah S, McNitt-Gray M, Rogers S et al: Computer-aided lung nodule diagnosis using a simple classifier. Proc Computer Assisted Radiology and Surgery 2004, pp952-955

〔9〕 Arimura H, Li Q, Korogi Y et al: Development of CAD scheme for automated detection of intracranial aneurysms in magnetic resonance angiography. Proc Computer Assisted Radiology and Surgery 2004, pp1015-1020

〔10〕 平野　靖，長谷川純一，鳥脇純一郎，他：3 次元胸部 X 線 CT 像からのインタラクティブな肺腫瘤領域の抽出と良悪性鑑別への応用．電子情報通信学会論文誌 D-II **J87-D-II**(1): 237-247, 2004

〔11〕 Kawata Y, Niki N, Ohmatsu H et al: Computer-aided differential diagnosis of pulmonary nodules based on a hybrid classification approach. Proc SPIE Medical Imaging **4322**: 1796-1806, 2001

〔12〕 Swensen SJ, Jett JR, Sloan JA et al: Screening for Lung Cancer with Low-DoseSpiral Computed Tomography. Am J Respir Crit Care Med **65**: 508-513, 2002

〔13〕 池添潤平，村田喜代史 編：胸部の CT．メディカル・サイエンス・インターナショナル，1998

〔14〕 森田洋介，宮下和人，平野　靖，他：胸部 X 線 CT 像からの炎症性小結節認識のための 3 次元形状特徴量の開発．信学技報 **MI2003-111**: 79-84, 2004

〔15〕 大津展之，栗田多喜夫，関田　巌：パターン認識ー理論と応用ー．朝倉書店，1996

〔16〕 末永康仁，鳥脇純一郎，福村晃夫：濃淡図形処理のための Range フィルタとその応用．信学論 D **57-D**(1): 23-30, 1974

〔17〕 早瀬陽介，草薙 卓，目加田慶人，他：図形形状特徴と最小方向差分フィルタによる3次元胸部CT像からの小結節検出．信学技報 (MI) **MI2002-90**: 59-64, 2003
〔18〕 重本加奈恵，滝沢穂高，山本眞司，他：3次元結節・血管モデルとテンプレートマッチングを用いた胸部X線CT画像からの結節陰影の高速認識．Med Imag Tech **21**(2): 147-156, 2003
〔19〕 Oda T, Saita S, Kubo M et al: Nodule detection algorithm based on multislice CT images for lung cancer screening. Proc SPIE Medical Imaging **5370**: 1083-1090, 2004
〔20〕 丹後敏郎，山岡和枝，高木晴良：ロジスティック回帰分析－SASを利用した統計解析の実際－．朝倉書店，東京，1996
〔21〕 D.R.Cox 著，後藤昌司，畠中駿逸，田崎武信 訳：二値データの解析．朝倉書店，東京，1980
〔22〕 鳥脇純一郎：認識工学．コロナ社，東京，1992

［付 録］

A. ロジスティック回帰モデルへの当てはめ

本文では，以下のようにした〔20, 21〕．ある結節に対する特徴量ベクトル $\boldsymbol{x}=(x_1, x_2, \cdots, x_5, x_{61}, x_{62})^{\mathrm{T}}$ が与えられたとき，その結節が炎症性小結節である事後確率 $P(\text{inflam.}|\,\boldsymbol{x})$ は

$$P(\text{inflam.}|\,\boldsymbol{x})=\frac{1}{1+\exp(-Z)} \tag{A1}$$

と表現される．ただし，Z はパラメータベクトル $\boldsymbol{\beta}=(\beta_1, \beta_2, \cdots, \beta_5, \beta_{61}, \beta_{62})^{\mathrm{T}}$ を用いて次式で定義される．

$$Z=\beta_1 x_1+\beta_2 x_2+\cdots \beta_5 x_5+\beta_{61} x_{61}+\beta_{62} x_{62} \tag{A2}$$

B. ロジスティック判別

判別には，カテゴリの事前確率が等しいと仮定したロジスティック判別を用いる．すなわち，特徴量ベクトルが $\boldsymbol{x}$ である結節に対して上記の $P(\text{inflam.}|\,\boldsymbol{x})$ を計算し，$P(\boldsymbol{x})>0.5$ であれば炎症性小結節，そうでないならその他の結節と判別する．パラメータベクトル $\boldsymbol{\beta}$ は学習サンプルから最尤推定により決定したものを用いる．最尤推定では，次式の対数尤度 $L(\boldsymbol{\beta})$ を最大化するパラメータベクトル $\boldsymbol{\beta}$ を決定する．

$$L(\boldsymbol{\beta})=\log\left\{\prod_{i=1}^{n} P(\text{inflam.}|\,\boldsymbol{x}^{(i)})^{y^{(i)}}\left(1-P(\text{inflam.}|\,\boldsymbol{x}^{(i)})^{1-y^{(i)}}\right)\right\} \tag{A3}$$

ただし，添字 i は結節サンプルの番号，n は学習サンプルの総数，$P(\text{inflam.}|\,\boldsymbol{x}^{(i)})$ は結節 i が炎症性小結節である事後確率 $P(\text{inflam.}|\,\boldsymbol{x})$，$y^{(i)}$ は結節 i が炎症性小結節なら1，そうでないなら0となる変数である．

C. モデルの適合性

モデルの適合性を検証するには，規準化した残差

$$D_i=\frac{y^{(i)}-P(\text{inflam.}|\,\boldsymbol{x}^{(i)})}{\sqrt{P(\text{inflam.}|\,\boldsymbol{x}^{(i)})\left(1-P(\text{inflam.}|\,\boldsymbol{x}^{(i)})\right)}} \tag{A4}$$

がモデル適合時に，標本の大きさが大きくなるにしたがって漸近的に標準正規分布に従うことを利用する．

D. 変数の有意性

特徴量 x_k が有意な寄与をするか否かは，帰無仮説 H_0 を“(A2)式における β_k は0と等しい”とした仮説検定で判断される．具体的には，任意の特徴量 x_k に対応する β_k の値を0としたとき，$\beta_k=0$ とする前後の $\boldsymbol{\beta}$ の最尤推定値をそれぞれ $\boldsymbol{\beta}'$, $\boldsymbol{\beta}''$ とし，$\boldsymbol{\beta}'$, $\boldsymbol{\beta}''$ の次元数をそれぞれ a, b とすると，

$$\chi_0^2=2\{L(\boldsymbol{\beta}')-L(\boldsymbol{\beta}'')\} \tag{A5}$$

は自由度 $(a-b)$ の x^2 分布に従う．(A5)式の値が自由度 $(a-b)$ の x^2 分布における有意水準 α での棄却域に属するとき，帰無仮説 H_0 は棄却でき，該当する変数が有意水準 α で有意であると判断できる．

Method for Identifying Inflammatory Nodules from Lung Nodules Extracted from Chest X-ray CT Images for Computer-Aided Diagnosis

Kazuto MIYASHITA[*1], Yasushi HIRANO[*1], Yoshito MEKADA[*2], Hiroshi MURASE[*1], Jun-ichi HASEGAWA[*2], Junichiro TORIWAKI[*2], Nobuhiko SEKI[*3], Kenji EGUCHI[*3], Tsuneo MATSUMOTO[*4], Hironobu OHMATSU[*5], Hiroshi MOGAMI[*6], Masao NAKATA[*7]

[*1] *Nagoya University*
[*2] *Chukyo University*
[*3] *Tokai University*
[*4] *Yamaguchi University*
[*5] *National Cancer Center Hospital East*
[*6] *National Hospital Organization Shikoku Cancer Center*
[*7] *Kawasaki Medical School*

In this paper, we propose a method for identifying a type of benign nodules known as "inflammatory nodules" seen in thin-slice chest X-ray CT images. It may be possible to determine whether such nodules are benign based on the observation of medical findings without biopsy or follow-up. We quantified such medical findings using six features. Four features were elated to the nodule itself (ratio of the linear part of the boundary to the entire boundary, diameter, morphological complexity, and variation in CT values within the nodule) and two features were related to the relationships between the nodule and the chest wall near the nodule (distance between them and the presence of interlobular septa). In order to identify inflammatory nodules, we used a logistic regression model. This method was applied to 83 patients with small, solid nodules, including 44 patients with inflammatory nodules. The accuracy of identification was 80%. We also performed hypothesis testing for the significance of the proposed features. It was confirmed that two of the features (diameter and variation in CT values within the nodule) were significant.

Key words: Inflammatory nodule, Benign/malignant discrimination, Chest X-ray CT images, Logistic regression analysis, Computer-aided diagnosis
Med Imag Tech **23** (3): 161-171, 2005

宮下和人（みやした　かずと）
2004年名古屋大学博士課程前期課程（情報工学専攻）了．現在，㈱日立 IE システムソフト設計部．在学中は胸部 X 線 CT 像に対する診断支援に関する研究に従事．

平野　靖（ひらの　やすし）
1995 年名大・工・電子情報卒．1997 年同大大学院博士課程前期課程（電子情報学専攻）了．1999 年同大大学院博士課程後期課程（情報工学専攻）了．2000 年同大大学院工学研究科助手．2002年同大情報連携基盤センター助手．2004年同大情報連携基盤センター助教授．博士（工学）．1998 年 4 月より 1999 年 11 月まで日本学術振興会特別研究員（DC2），1999 年 12 月より 2000 年 3 月まで日本学術振興会特別研究員（PD）．3次元画像処理とその肺腫瘤の良悪性鑑別への応用に関する研究に従事．電子情報通信学会学会，日本生体医工学会，コンピュータ支援画像診断学会，および IEEE 各会員．1998 年度本学会論文賞．

目加田慶人（めかだ　よしと）
1991 年名大・工・情報卒．1996 年同大学大学院博士後期課程修了．1996年宇都宮大学工学部情報工学科助手．2001年名古屋大学大学院工学研究科情報工学専攻助教授，2004 年より中京大学生命システム工学部教授，現在に至る．画像処理・パターン認識とその医用応用，信号処理などの研究に従事．博士（工学）．電子情報通信学会，IEEE，コンピュータ支援画像診断学会，胸部 CT 検診研究会各会員．

村瀬　洋（むらせ　ひろし）
1978 年 名大・工・電気卒．1980 年 同大学院修士課程了．同年日本電信電話公社（現 NTT）入社．1992 年から 1 年間米国コロンビア大客員研究員．2003年から名古屋大学大学院情報科学研究科教授．現在に至る．文字・図形認識，コンピュータビジョン，マルチメディア認識の研究に従事．工博．1994 年 IEEE-CVPR 最優秀論文賞，2001 年高柳記念奨励賞，2002 年電子情報通信学会業績賞，2003 年文部科学大臣賞他受賞，2004 年 IEEE Trans.MM 論文賞，他受賞．電子情報通信学会，情報処理学会，IEEE 各会員．

長谷川純一（はせがわ　じゅんいち）

1974 年名古屋大学工学部電気学科卒. 1979年同大学大学院博士課程了. 同年名古屋大学工学部助手, 1986 年同講師. 1987 年中京大学教養部助教授, 1992年同情報科学部教授, 2004 年同生命システム工学部教授. 工博. パターン認識, 画像理解とそれらの医療・スポーツへの応用に関する研究に従事. 日本生体医工学会, コンピュータ支援画像診断学会, 電子情報通信学会, 情報処理学会などの会員. 1991, 1996, 1998年度本学会論文賞.

鳥脇純一郎（とりわき　じゅんいちろう）

1962年名大・工・電子卒. 1967年同大大学院博士課程了. 同年4月名古屋大学工学部助手. 以降, 1970年助教授, 1974年名古屋大学大型計算機センター助教授, 1980年豊橋技術科学大学情報工学系教授, 1983年名古屋大学工学部電子工学科教授, 1985年4月同情報工学科(1994年4月より大学院工学研究科情報工学専攻）教授, 2003年4月中京大学情報科学部教授を経て, 2004年4月中京大学生命システム工学部教授, 名古屋大学名誉教授. 工博. パターン認識, 画像処理, グラフィックスおよびそれらの医学情報処理への応用に関する研究に従事. 著書「画像理解のためのディジタル画像処理 I, II」(昭晃堂).「パターン情報処理の基礎」(朝倉書店),「認識工学」(コロナ社),「3 次元ディジタル画像処理」(昭晃堂), 情報処理学会, 日本生体医工学会, コンピュータ支援画像診断学会, 人工知能学会, 画像電子学会, IEEE 各会員.

関　順彦（せき　のぶひこ）

1994 年年防衛医科大・医卒. 同大学第3内科を経て, 1996 年大阪医科大学第一内科で一般呼吸器診療に従事. その後, 2000年国立病院四国がんセンターで呼吸器内科レジデント, 2002 年東海大学病院呼吸器内科助手を経て, 2005 年より同腫瘍内科助手として肺癌の治療と画像診断に従事. 現在, 末梢型肺腺癌の発生と進展過程につきCT画像と分子生物学的アプローチを主体として研究中.

江口研二（えぐち　けんじ）

1973 年慶応大学医学部卒, 同放射線科教室を経て, 1975年から国立がんセンター呼吸器レジデント, 1979 年同病院内科, 1987年米国 Mayo Clinic, Visiting Physician, 国立がんセンター病院内科医長, 1997 年国立病院四国がんセンター副院長を経て, 2002 年 2 月から東海大学医学部医学科内科学系呼吸器内科 教授. 専門は, 胸部腫瘍の画像診断と薬物療法である. 肺癌の低線量ヘリカルCT検診や早期診断法について現場での技術向上の重要性を認識し, コンピュータによる診断支援技術の開発を注目している. 日本内科学会, 呼吸器学会, 肺癌学会, 気管支学会, 臨床腫瘍学会, 癌学会, 癌治療学会, 緩和医療学会などに所属している.

松本常男（まつもと　つねお）

1976 年山口大学医学部卒業, 医学博士(山口大). 助手, 講師を経て, 1995 年より山口大学医学部放射線科（現 構造制御病態学・放射線医学講座）助教授. 1990 年より1年間シカゴ大学カートロスマン研究所にて胸部単純写真のコンピューター支援診断についての研究で留学. 専門は画像診断, とくに胸部画像診断. 肺がん集団検診, 胸部画像における CAD などの研究に従事. 腫瘍学を画像から解析することを目標に研究している. 日本放射線学会, 日本呼吸器学会, 日本肺癌学会, 日本気管支学会, 日本結核病学会会員などに所属.

大松広伸（おおまつ　ひろのぶ）

1988 年旭川医科大学医学部卒. 同年同大学第 1 内科入局. 呼吸器科学, 循環器病学の臨床研究に従事. 1990 年国立がんセンター肺内科レジデントとして, 肺がんの診断, 治療の臨床研究に従事. 1993 年国立がんセンター東病院呼吸器科にて, 肺がんの診断, 治療の臨床研究に従事. 現在, 末梢型肺がんの早期診断について, CT 画像を中心に研究中.

最上　博（もがみ　ひろし）

1980 年愛媛大学医学部卒. 現在, 国立病院機構四国がんセンター放射線診断科医長. 画像診断に関する研究に従事.

中田昌男（なかた　まさお）

1985 年岡山大学医学部卒, 同年岡山大学医学部大学院第二外科学教室入学, 1990年寺岡記念病院外科, 1993 年国立病院四国がんセンター外科, 2003 年川崎医科大学（胸部心臓血管）助教授. 小型肺癌の手術適応に関する研究に従事.

*　　*　　*

Development of a Novel Computer-Aided Diagnosis System for Automatic Discrimination of Malignant From Benign Solitary Pulmonary Nodules on Thin-Section Dynamic Computed Tomography

Kiyoshi Mori, MD, Noboru Niki, PhD,† Teturo Kondo, MD,* Yukari Kamiyama, MD,* Teturo Kodama, MD,* Yoshiki Kawada, PhD,† and Noriyuki Moriyama, MD‡*

Objectives: As an application of the computer-aided diagnosis of solitary pulmonary nodules (SPNs), 3-dimensional contrast-enhanced (CE) dynamic helical computed tomography (HCT) was performed to evaluate temporal changes in the internal structure of nodules to differentiate between benign nodules (BNs) and malignant nodules (MNs).

Methods: There were 62 SPNs (35 MNs and 27 BNs) included in this study. Scanning (2-mm collimation) was performed before and 2 and 4 minutes after CE dynamic HCT. The CT data were sent to a computer, and the pixels inside the nodule were characterized in terms of 3 parameters (attenuation, shape index, and curvedness value).

Results: Based on the CT data at 4 (MN: 1.81–27.1, BN: −42.8 to −3.29) minutes after CE–dynamic HCT, a score of 0 or higher can be assumed to indicate an MN.

Conclusions: Three-dimensional computer-aided diagnosis of the internal structure of SPNs using CE dynamic HCT was found to be effective for differentiating between BNs and MNs.

Key Words: coin lesion, pulmonary, computer-aided design, lung neoplasms, radiographic image enhancement, tomography, x-ray computed

(*J Comput Assist Tomogr* 2005;29:215–222)

The morphologic imaging diagnosis of solitary pulmonary nodules (SPNs) has been performed based on qualitative findings, mainly in computed tomography (CT) images, identified by diagnosticians when evaluating the characteristics of the nodule's margins, internal structure, and relations to surrounding structures.[1–3] The interpretation of these findings tends to differ, however, depending on the person performing the diagnosis, and diagnostic standards for differentiating between benign nodules (BNs) and malignant nodules (MNs) have yet to be established. The quantitative diagnosis of such lesions has been attempted based on the measurement of attenuation in the nodule. Attenuation has been used for the objective assessment of the internal structure of nodules and for the differential diagnosis of BNs and MNs.[4] There have also been reports on the use of contrast medium to evaluate changes in attenuation in nodules over time to differentiate between BNs and MNs.[5–8] In these studies, however, the attenuation in the nodules was measured in only a few slices. Moreover, because the region of interest (ROI) within the lesion was specified manually, the attenuation obtained showed a large degree of variation in different slices.

The use of helical scanning has facilitated the acquisition of volume data for the entire lesion, making it possible to analyze these image data using a computer.[9–11] In the present study, images of the entire lesion were obtained using contrast-enhanced (CE) dynamic helical computed tomography (HCT), and the changes in the density of the lesion over time were calculated with a computer and quantified in a 3-dimensional (3D) perspective for the differential diagnosis of BNs and MNs.

SUBJECTS AND METHODS

CT Imaging Conditions

Computed tomography images were obtained using an Xpress/SX system (Toshiba Corporation, Tokyo, Japan). The scanning parameters were a patient couch-top movement speed of 2 mm/s, a beam width of 2 mm, a tube voltage of 120 kV, a tube current of 200 mA, 1-second scanning, and an ROI of 200 mm. A total of 100 mL nonionic contrast medium (Iopamiron 300 Syringe; Nihon Schering, Tokyo, Japan) was injected at a rate of 2 mL/s using an autoinjector through a peripheral forearm vein. With the patient placed in the supine position and receiving supplemental oxygen via a nasal cannula (2 L/min), helical scanning covering the entire lesion (40–50 mm) was performed 3 times during breath-holding (before enhancement and 2 and 4 minutes after the start of

Received for publication August 10, 2004; accepted January 3, 2005.
From the *Department of Thoracic Diseases, Tochigi Cancer Center, Tochigi, Japan, †Department of Optical Science, University of Tokushima, Tokushima, Japan, and ‡Department of Radiology, National Cancer Center, Tokyo, Japan.
Supported in part by a grant-in aid for cancer research from the Ministry of Health and Welfare of Japan and the Second-Term Comprehensive 10-Year Strategy for Cancer Control.
Reprints: Kiyoshi Mori, Department of Thoracic Diseases, Tochigi Cancer Center, 4-9-13 Younan, Utsunomiya, Tochigi 320-0834, Japan (e-mail: kmori@tcc.pref.tochigi.jp).

contrast injection). Images were reconstructed at 1-mm intervals using a 180° algorithm.

Evaluation of CT Images

CT Image Processing

The tumor lesion was extracted from the thin-section CT images and then reconstructed to obtain a 3D CT image of the tumor.[9] The density was then calculated by characterizing the pixels inside the extracted nodule in terms of 3 parameters (attenuation, shape index, and curvedness value). Based on the calculated density values within each nodule before enhancement and 2 and 4 minutes after the start of injection, a linear discriminant function score was obtained for each time point.

Extraction of Lesions

After the reconstruction of 3D images from the thin-section CT images, ROIs containing the nodules were extracted from these images (Fig. 1). Using a deformable surface model, the nodules were then extracted from these ROIs.[9,12] In some cases, the nodules were located adjacent to the pleura. In such cases, preprocessing was required for extracting the region of the lung fields to separate the pleura from the nodules.[10] The segmentation of the nodule was based on a thresholding technique and selection of object connected components. In the present study, a method based on the deformable surface model proposed by Caselles et al[12] was used for extracting nodular regions with various density distributions.[10] This approach is based on deforming 3D surfaces, represented by level sets, toward the nodule boundary to be extracted in the 3D images. It automatically handles the changes in the surface topology during deformation. In this method, the nodular region is extracted by placing the initial curved surface within the nodule and then transforming the surface to conform to the margins of the nodule using a formula for the curved surface.[12] In this way, excessive overflow of blood vessels and bronchi relative to the curved surface can be prevented by adjusting the end points for curved surface transformation.[10]

Display and Assessment of Characteristic Values Within the Lesion

The pixels in the ROI, including the nodule, were expressed locally using a combination of 3 parameters: the attenuation, shape index, and curvedness value (Figs. 2, 3).[13,14]

The shape index and curvedness value are defined by the 3D curvature of the curved surface. The shape index ranges from 0 to 1. As the shape index approaches 0, the surface becomes increasingly convex (peak surface), and as the shape index approaches 1, the surface becomes more concave (pit surface). Thus, subtle curved surface structures can be expressed in numeric form. The curvedness value reflects the degree of curvature and ranges from 0 to 1. As the curvedness value approaches 0, the surface becomes flatter with less curvature. The concepts of the shape index and curvedness value can be easily understood when these 2 parameters are used for the curved surface of the tumor margins (boundary structures between the periphery of the nodule and the surrounding lung). These parameters, the shape index and curvedness value, obtained from the 3D curvature represent the concavoconvex structure of the curved surface and the degree of curvature of the curved surface, which are both determined from the relations between the target pixels and their adjacent pixels. These parameters can be regarded as indices of the uneven distribution of attenuation within the nodule. The histograms of the shape index, curvedness value, and attenuation within the nodule are obtained, and the scale of each histogram serves as a histogram characteristic value.[14] The Fisher linear discriminant classifier is commonly used in pattern classification and is an optimal classifier when the sample distributions are multivariate normal with equal covariance matrices.[15] The linear discriminant classifier was designed by using the histogram features. A leave-one-out procedure was performed to provide a less biased estimation of the performance of the linear discriminant classifier.[16] In this procedure, 1 nodule image is left out from the classifier design group and a linear discriminant function is formulated using the design group. The discriminant score is computed for the case that is left out by using the linear discriminant function obtained. This process cycles through the data set until every

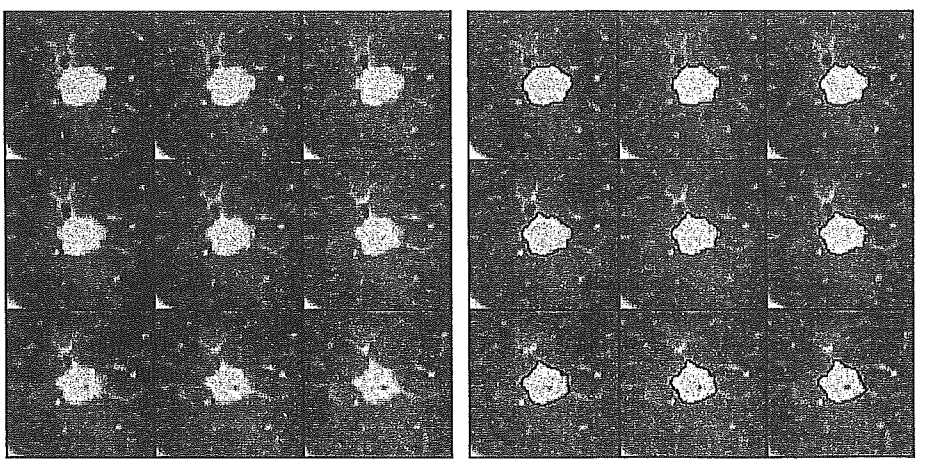

FIGURE 1. Extraction of a pulmonary nodule (case 8).

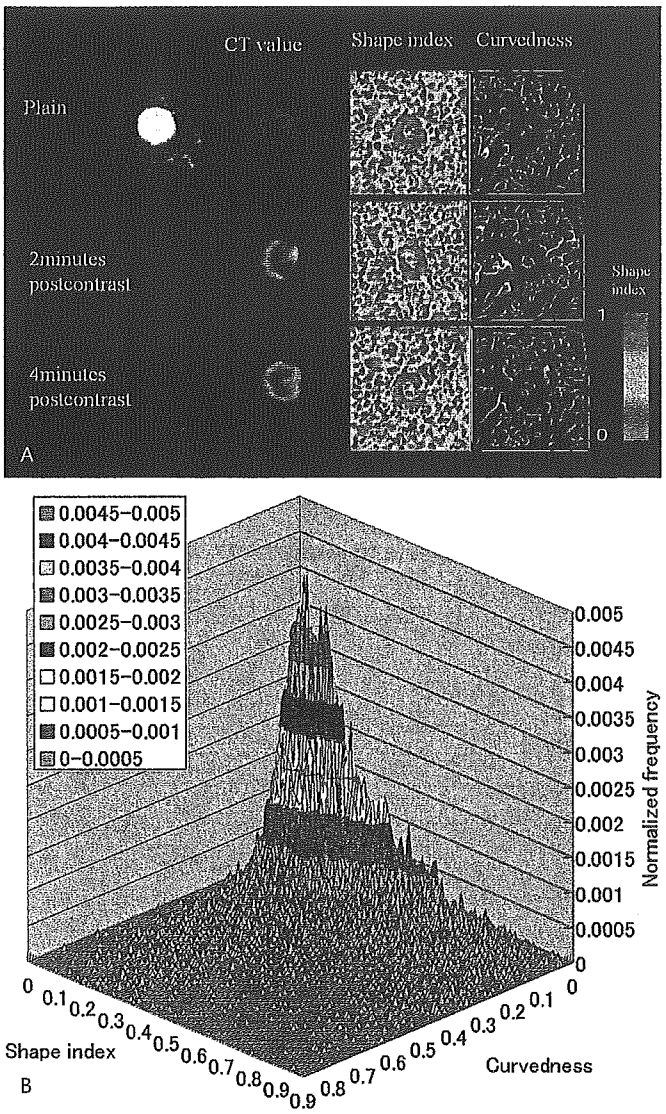

FIGURE 2. A, Characteristic values for a benign nodule (BN; case 37). B, Shape spectra showing a combination of the shape index and curvedness value 4 minutes after contrast enhancement. The *z* axis shows frequency. Most pixels inside a BN have a shape index close to 0 and a low curvedness value. This indicates that pixels inside a BN are mainly of the peak surface type with a smoothly curved surface.

nodule image is used. The overall evaluation time was approximately 4 minutes, including selection of the ROI from the CT images, extraction of the nodule, characterization of the pixels inside the nodule, and calculation of the linear discriminant function scores.

In the present study, each linear discriminant function score was computed from the shape index, curvedness value, and attenuation at each time point: before contrast enhancement and 2 and 4 minutes after the start of enhancement. The malignancy of SPNs was then retrospectively analyzed based on the scores obtained.

In addition, receiver operating characteristic curves were used to evaluate the effectiveness of the linear discriminant score in differentiating between BNs and MNs. Statistical significance was assessed using the unpaired Student *t* test.

Subjects

The subjects in this study were 72 consecutive patients who had undergone chest CT for the detailed examination of SPNs at our department from February 1998 to April 2000. They had only 1 target nodule by CT. Ten patients were not included in the assessment in this study, because CT images of the entire lesion could not be obtained over time (before contrast enhancement and 2 and 4 minutes after contrast enhancement) in these patients because of patient respiratory motion. The remaining 62 patients were evaluated. The mean

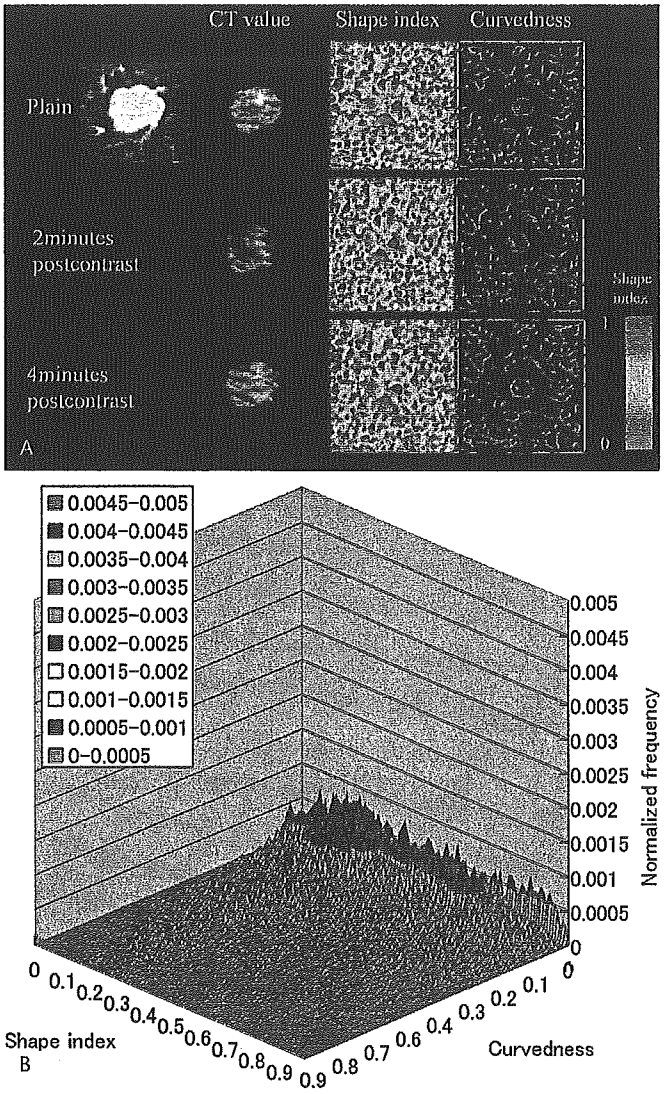

FIGURE 3. A, Characteristic values for a malignant nodule (MN; case 8). B, Shape spectra showing a combination of the shape index and curvedness value 4 minutes after contrast enhancement. Compared with a benign nodule (BN), pixels inside an MN show a wide distribution of shape index values, ranging from 0 to 1, and a high curvedness value. This indicates that pixels inside an MN tend to have pixels other than the peak surface type compared with a BN.

diameter of all nodules was 14 mm (range: 5–25 mm), with a mean diameter of 17 mm (range: 8–25 mm) for MNs and 10 mm (range: 5–17 mm) for BNs. These nodules were classified as 35 malignant lesions (primary lung carcinoma in 33 patients [adenocarcinoma in 31 patients and squamous cell carcinoma in 2 patients] and metastatic pulmonary tumor in 2 patients [breast cancer and colon cancer in 1 patient each]; Table 1) and 27 benign lesions (nonspecific benign lesion in 16 patients, granuloma in 4 patients, hamartoma in 3 patients, organized pneumonia in 1 patient, tuberculoma in 1 patient, pulmonary infarction in 1 patient, and pneumonia in 1 patient; Table 2). The primary lung carcinomas were surgically resected in 29 patients, with the exception of 4 patients with adenocarcinoma. The pathologic stage of the resected tumor was histopathologically graded as stage I in 24 patients, stage II in 1 patient, and stage III in 4 patients. The degree of differentiation of the adenocarcinomas in 27 patients was highly differentiated in 11 patients, moderately differentiated in 14 patients, and poorly differentiated in 2 patients. Metastatic lung tumors were found in these 2 patients based on CT fluoroscopy-guided biopsy. Benign lesions were surgically resected in 4 patients (granuloma, organized pneumonia, tuberculoma, and pulmonary infarction) and identified based on CT fluoroscopy-guided biopsy in 6 patients (hamartoma in 3 patients and granuloma in 3 patients). The nodule disappeared in 1 patient with pneumonia, whereas the remaining 16 patients were diagnosed with a nonspecific benign lesion based on the shape of the lesion and changes in

TABLE 1. Characteristics and Quantitative Characterization of MNS

Patient No.	Age (y)	Sex	Diameter (mm)	Lobe	Linear Discriminant Function			Diagnosis
					Non-Enhanced	2 Min*	4 Min*	
1	5	F	18	RU	1.49	4.42	17.42	W/d AD
2	48	F	18	LU	1.64	10.92	16.95	W/d AD
3	77	M	12	LU	2.4	7.14	24.9	AD
4	68	F	22	RL	4.01	15.77	21.8	M/d AD
5	68	M	11	LU	0.85	6.77	8.18	M/d AD
6	54	F	22	LL	1.96	13.29	14.84	Breast matastasis
7	63	M	12	RU	1.41	9.72	14.77	W/d AD
8	63	M	17	RL	2.25	2.65	9.38	M/d AD
9	55	F	18	LU	3.07	12.34	19.49	M/d AD
10	44	M	15	RU	4.65	4.97	11.71	M/d AD
11	61	F	20	RL	3.21	10.01	17.65	W/d AD
12	84	M	19	LU	3.24	11.07	13.36	AD
13	57	M	15	RU	1.88	9.82	21.61	M/d AD
14	71	M	20	LU	1.11	9.83	13.27	AD
15	61	M	13	RM	1.99	14.51	12.78	Colon matastasis
16	51	F	8	LU	0.93	1.58	9.09	W/d AD
17	51	M	18	LU	3.29	13.02	9.37	P/d AD
18	67	M	15	RU	0.89	12.23	14.58	M/d AD
19	62	F	11	RU	0.87	2.39	22.01	W/d AD
20	61	F	25	RM	1.58	9.56	8.77	W/d AD
21	49	F	19	RM	3.16	13.22	22.45	M/d AD
22	63	F	14	LU	1.32	11.5	9.56	W/d AD
23	45	M	12	RU	1.25	0.58	5.44	M/d AD
24	52	M	18	LU	3.4	9.82	13.59	M/d AD
25	56	F	13	RU	0.28	8.12	17.16	W/d AD
26	53	M	24	RU	2.77	14.89	22.35	M/d AD
27	65	F	23	LU	4.28	16.62	27.11	M/d AD
28	71	F	10	RU	−2.16	5.13	5.27	W/d AD
29	66	F	19	LU	2.68	6.95	18.72	P/d AD
30	40	F	19	RL	2.56	5.87	17.62	M/d AD
31	77	F	16	RU	−0.48	5.56	1.81	M/d AD
32	66	M	15	LL	2.26	23.14	2.95	AD
33	80	M	11	RL	0.13	2.19	22.44	M/d AD
34	68	F	19	RU	5.01	14.78	20.36	W/d AD
35	58	F	24	RL	3.25	15.25	22.56	M/d AD

*Time after administration of contrast agent.

AD indicates adenocarcinoma; F, female; LLL, left lower lobe; LUL, left upper lobe; M, male; M/d, moderately differentiated; P/d, poorly differentiated; RLL, right lower lobe; RML, right middle lobe; RUL, right upper lobe; SQ, squamous cell carcinoma; W/d, well differentiated.

TABLE 2. Characteristics and Quantitative Characterization of BNS

Patient No.	Age (y)	Sex	Diameter (mm)	Lobe	Linear Discriminant Function			Diagnosis
					Non-Enhanced	2 Min*	4 Min*	
36	51	F	9	RU	−4.24	−12.77	−11.83	Nonspecific†
37	57	F	10	LU	−1.03	−14.41	−10.29	Hamartoma
38	56	F	15	LU	1.82	−7.56	−3.29	Granuloma
39	65	F	8	RM	−4.68	−11.38	−10.45	Nonspecific†
40	52	F	10	LU	−0.64	−6.93	−17.34	Nonspecific†
41	72	F	10	LL	1.25	3.56	−10.7	Granuloma
42	61	M	7	RL	−3.71	−9.15	−16.22	Nonspecific†
43	70	M	9	RU	−1.21	−7.04	−18.99	Organizing/pneumonia
44	68	F	17	LU	0.97	−3.98	−17.41	Pulmonary/infarction
45	47	F	5	RU	−5.3	−18.14	−32.32	Granuloma
46	56	F	12	RU	−0.85	−18.61	−10.88	Tuberculoma
47	59	F	9	LL	−4.81	−9.74	−19.01	Nonspecific†
48	62	F	12	RM	2.14	−5.63	−4.22	Nonspecific†
49	61	F	6	RM	−5.3	−9.09	−23.16	Nonspecific†
50	60	F	8	RU	−3.53	−18.94	−42.75	Nonspecific†
51	68	F	12	RU	0.54	−19.49	−15.17	Nonspecific†
52	67	M	6	RU	−5.3	−12.58	−21.51	Nonspecific†
53	68	M	8	LL	−4.28	−5.13	−27.26	Nonspecific†
54	64	M	8	RM	−3.82	−7.12	−19.13	Hamartoma
55	70	F	15	RM	2.57	−12.02	−38.67	Nonspecific†
56	60	M	15	RL	−0.49	−5.23	−11.81	Nonspecific†
57	53	F	15	RU	1.2	0.83	−7.36	Granuloma
58	73	M	10	LL	−0.08	0.89	−4.16	Pneumonia
59	72	M	17	LL	−3.24	−9.6	−9.89	Nonspecific†
60	58	M	7	RU	−4.94	−14.21	−10.37	Hamartoma
61	45	M	7	LL	−5.3	−11.81	−6.44	Nonspecific†
62	43	F	8	RL	−3.47	−9.39	−14.15	Nonspecific†

*Time after administration of contrast agent.
†The clinical diagnosis of a nonspecific benign lesion was based on no nodule growth for 2 years or longer.
F, female; LLL, left lower lobe; LUL, left upper lobe; M, male; M/d, moderately differentiated; P/d, poorly differentiated; RLL, right lower lobe; RML, right middle lobe; RUL, right upper lobe; W/d, well differentiated.

size during a follow-up observation period of 2 years or more.[4,17]

This study was approved by the ethical committee of our institution. Written informed consent was obtained from the patients.

RESULTS

Receiver operating characteristic curves were used to evaluate the effectiveness of the diagnostic method using the histogram characteristic values of the attenuation, curvedness value, and shape index to differentiate between BNs and MNs. Evaluation was performed for each parameter as well as for values obtained at different time points: before enhancement and 2 and 4 minutes after enhancement.

The areas under the ROC curve for the attenuation before, 2 minutes after, and 4 minutes after contrast enhancement were 0.58 ± 0.07, 0.69 ± 0.07, and 0.57 ± 0.08, respectively (Fig. 4A); those for the curvedness value were 0.78 ± 0.06, 0.83 ± 0.05, and 0.76 ± 0.06, respectively (see Fig. 4B); and those for the shape index were 0.90 ± 0.04, 0.89 ± 0.05, and 0.90 ± 0.04, respectively (see Fig. 4C). The results for evaluation of all 3 parameters combined were 0.91 ± 0.04, 0.99 ± 0.01, and 1.00, respectively (see Fig. 4D).

Evaluation based on all 3 parameters combined gave the best results. The changes in the linear discriminant function scores over time were analyzed for these combined parameters.

The mean scores before enhancement were −2.06 ± 2.70 (range: −5.3–2.57) for BNs and 2.09 ± 1.50 (range: −2.16–5.01) for MNs. Those at 2 and 4 minutes after enhancement were 9.59 ± 5.04 (range: 0.58–23.1) and 15.1 ± 6.50 (range: 1.81–27.1), respectively, for MNs (see Table 1) and −9.43 ± 5.94 (range: −19.5–3.56) and −16.1 ± 9.94 (range: −42.8 to −3.29), respectively, for BNs (see Table 2). The linear discriminant function scores for MNs were significantly higher than those for BNs at all 3 time points: before enhancement ($P < 0.001$), 2 minutes after enhancement ($P < 0.001$), and 4 minutes after enhancement ($P < 0.001$).

When a linear discriminant function score of 0 or higher was considered to indicate malignancy, there were 2 false-negative (FN) findings (cases 28 and 31) and 7 false-positive (FP) findings (cases 38, 41, 44, 48, 51, 55, and 57) before

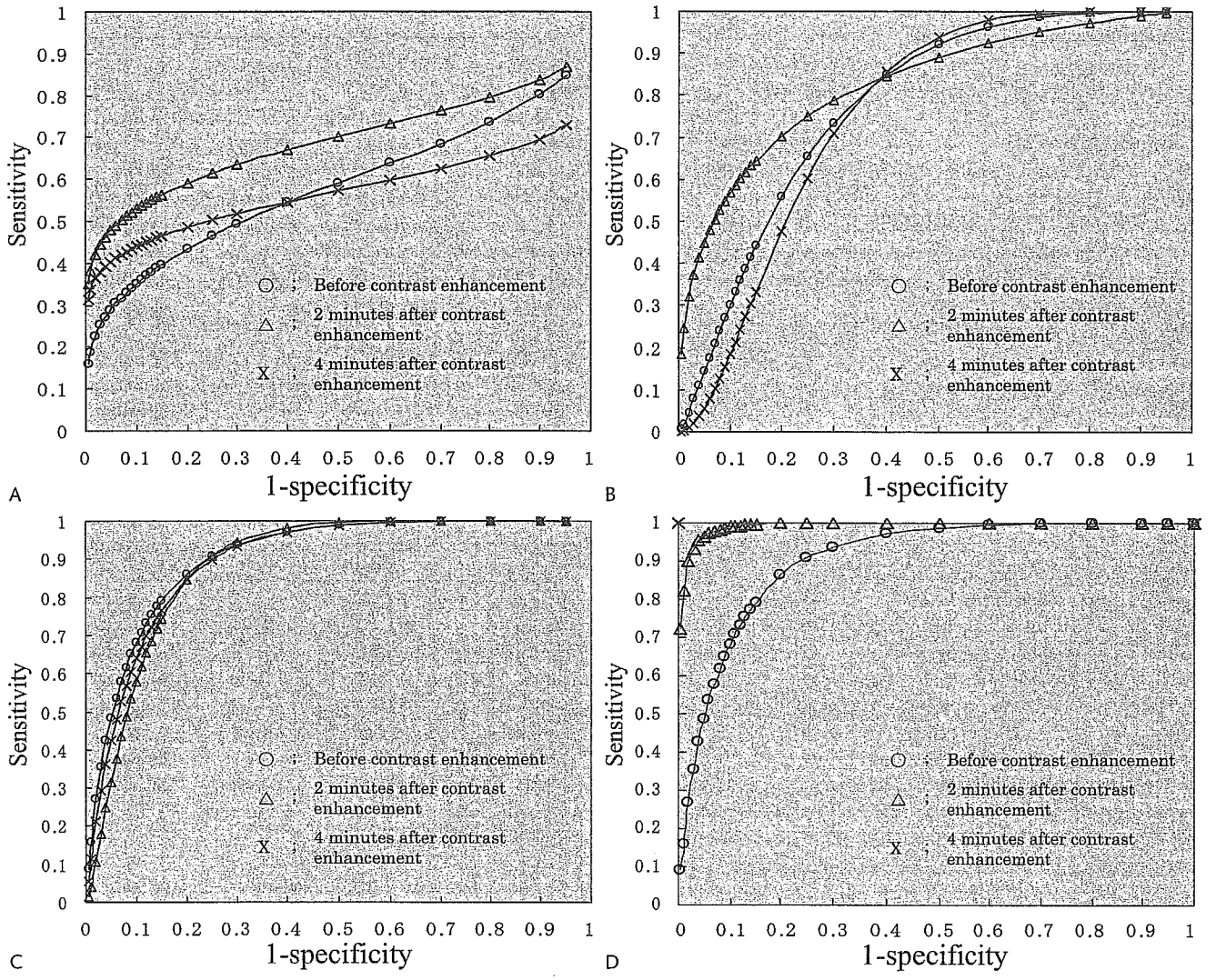

FIGURE 4. Receiver operating characteristic curves for each parameter used to differentiate between malignant and benign nodules. The open circles (○) are before contrast enhancement, and the open triangles (△) and crosses (x) are 2 and 4 minutes after contrast enhancement, respectively. A, Areas under the open circle (○), open triangle (△), and cross (x) curves for attenuation are 0.58 ± 0.07, 0.69 ± 0.07, and 0.57 ± 0.08, respectively. B, Areas under the open circle (○), open triangle (△), and cross (x) curves for curvedness value are 0.78 ± 0.06, 0.83 ± 0.05, and 0.76 ± 0.06, respectively. C, Areas under the open circle (○), open triangle (△), and cross (x) curves for shape index are 0.90 ± 0.04, 0.89 ± 0.05, and 0.90 ± 0.04, respectively. D, Areas under the open circle (○), open triangle (△), and cross (x) curves for the combination of all 3 parameters (attenuation, shape index, and curvedness value) are 0.91 ± 0.04, 0.99 ± 0.01, and 1.00, respectively.

enhancement, 0 FN findings and 3 FP findings (cases 41, 57, and 58) 2 minutes after enhancement, and 0 FN findings and 0 FP findings 4 minutes after enhancement. Sensitivity values were 94%, 100%, and 100%; specificity values were 74%, 89%, and 100%; and accuracy values were 85%, 92%, and 100%, respectively. Positive predictive values were 83%, 92%, and 100%, and negative predictive values were 91%, 100%, 100%, respectively.

DISCUSSION

The usefulness of diagnostic imaging, focusing mainly on CT, for the evaluation of SPNs has been reported by researchers at a number of medical institutions.[1–4] Several of them have also attempted to differentiate between benign and malignant lesions by using contrast medium and evaluating attenuation within nodules over time.[5–8] These studies were based on attenuation and contrast enhancement patterns obtained for only a few slices in which the nodule was demonstrated, however.

In the present study, the entire nodule was scanned using CE dynamic HCT, and changes in the density and characteristic values (attenuation, shape index, and curvedness value) within the nodule were calculated for 3D quantification with a computer to discriminate between benign and malignant lesions. Contrast-enhanced dynamic HCT in combination with

the computer-aided diagnosis may thus improve the differential diagnosis of BNs and MNs.

With regard to the evaluation and interpretation of the CT data on the lesion, conventional studies have focused only on the 2-dimensional assessment of attenuation and the enhancement patterns in a few slices. The results of these studies were simple and practical, identifying the factors effective for the differential diagnosis to be an observed contrast effect of 20 Hounsfield units (HU) or greater[5,6] or 15 HU or greater,[8] enhancement of the entire lesion,[5] and a high CT value ratio between the nodule and arteries.[7] One problem was that the attenuation was strongly affected by the slice selected or the position of the ROI in the lesion, which was set manually. In the present study, this problem was avoided by automatically extracting the lesion as 3D volume data.[9,12] In addition, the nodule was evaluated by calculating the characteristic values within the nodule using a computer and measuring the density using 3 parameters (attenuation, shape index, and curvedness value).[10] The results showed that evaluation based on the combination of all 3 parameters provided the best results. Using this analysis method, each pixel within a tumor is expressed locally using the attenuation and the shape index and curvedness obtained from the 3D curvature, and the entire lesion is then characterized as benign or malignant using the histogram characteristic values. When these 3 histogram characteristic values were compared with each another, the shape histogram characteristic value was found to be superior to the other 2 values. The combination of these 3 characteristic values provided even better results. It is thought that a more detailed characteristic value for the internal structure of a tumor can be obtained by expressing the internal structure as a combination of attenuation and 3D curvatures.

When a linear discriminant function score not less than 0 at 2 and 4 minutes after enhancement was considered to indicate malignancy, the results showed 0 FN findings and 3 FP findings at 2 minutes after enhancement and no FN or FP findings at 4 minutes. When a linear discriminant function score of 0 or higher was considered to indicate malignancy, benign and malignant lesions were distinguished in all the patients using the data obtained 4 minutes after enhancement. It was considered that the values at 2 minutes were affected by the degree of minute blood vessel density within the nodule and that the values at 4 minutes were affected by the rate of contrast medium flowing into the papillary vessels and interstitial tissues or by the volume of the interstitial tissues.[18] In summary, compared with the techniques used in previous studies, the method described in the present study permits lesions to be extracted with fewer manual operations and higher reproducibility and is based on 3D analysis using 3 parameters (attenuation, shape index, and curvedness value).

The limitations of the present study are as follows. Although the objective of this study was to evaluate the entire nodule, it was difficult to visualize the entire nodule over time, even when an HCT scanner was used. As a result, lesions could not be assessed in 10 patients. It is expected that this problem can be overcome by the introduction of multislice HCT scanners in the near future. In this study, the score was assessed at each time point (before contrast enhancement and 2 and 4 minutes after contrast enhancement). In a strict sense, these scores do not represent the changes in the density of the lesion over time. In the assessment of changes over time, it is important to acquire CT images in exactly the same slice at each time point. The changes over time can then be obtained by performing subtraction between the images before and after contrast enhancement. In practice, however, it is difficult to acquire exactly the same slice at each time point because of the patient's respiratory motion. We are currently working to develop a new algorithm to overcome this problem. When this algorithm is complete, we plan to assess the changes in contrast medium density in lesions over time using subtraction.

In the future, CT-based lung cancer screening is expected to become more widely accepted, resulting in the detection of a larger number of SPNs.[19,20] Therefore, it is likely to become increasingly important to determine whether these lesions are benign or malignant based on evaluation of the images obtained.

Contrast-enhanced dynamic HCT was used for the computer-aided diagnosis of SPNs in the present study. The data obtained using this imaging technique permit the internal structure of lesions to be quantified in a 3D manner and evaluated over time. The results showed that this method is effective for differentiating between BNs and MNs. In the future, further prospective studies should be conducted based on the results reported here and standards for the evaluation of lesions using computer-aided analysis should be established.

REFERENCES

1. Mori K, Saitou Y, Tominaga K, et al. Small nodular lesions in the lung periphery: new approach to diagnosis with CT. *Radiology.* 1990;177: 843–849.
2. Kuriyama K, Tateishi R, Doi O, et al. CT-pathologic correlation in small peripheral lung cancers. *AJR Am J Roentgenol.* 1987;149:1139–1143.
3. Zwirewich CV, Vedal S, Miller RR, et al. Solitary pulmonary nodule; high-resolution CT and radiologic pathologic correlation. *Radiology.* 1991;179:469–476.
4. Siegelman SS, Khouri NF, Leo FR, et al. Solitary pulmonary nodules: CT assessment. *Radiology.* 1986;160:307–312.
5. Yamashita K, Matsunobe S, Tsuda T, et al. Solitary pulmonary nodule: preliminary study of evaluation with incremental dynamic CT. *Radiology.* 1995;194:399–405.
6. Swensen SJ, Brown LR, Colby TV, et al. Lung nodule enhancement at CT; prospective findings. *Radiology.* 1996;201:447–455.
7. Zhang M, Kono M. Solitary pulmonary nodules: evaluation of blood flow patterns with dynamic CT. *Radiology.* 1997;205:471–478.
8. Swensen SJ, Viggiano RW, Midthun DE, et al. Lung nodule enhancement at CT: multicenter study. *Radiology.* 2000;214:73–80.
9. Kawata Y, Niki N, Ohmatsu H, et al. Quantitative surface characterization of pulmonary nodules based on thin-section CT images. *IEEE Trans Nucl Sci.* 1998;45:2132–2138.
10. Kawata Y, Niki N, Mori K, et al. Curvature based analysis of internal structure of pulmonary nodules using thin-section CT images. *Proc IEEE Int Conf Image Processing.* 1998;3:851–855.
11. Armato SG, Li F, Giger ML, et al. Lung cancer: performance of automated lung nodule detection applied to cancers missed in a CT screening program. *Radiology.* 2002;225:685–692.
12. Caselles V, Kimmel R, Sapiro G, et al. Minimal surfaces based object segmentation. *IEEE Trans Pattern Anal Mach Intell.* 1997;19:394–398.
13. Koenderink JJ, van Doorn AJ. Surface shape and curvature scales. *Image Vis Comput.* 1992;10:557–565.

14. Dorai C, Jain AK. COSMOS-A representation scheme for 3D free-form objects. *IEEE Trans Pattern Anal Mach Intell.* 1997;19:1115–1130.
15. Duda RO, Hart PE. Pattern classification and scene analysis. In: Rosen CA, ed. *Linear Discriminant Functions*. New York: John Wiley & Sons; 1973:130–188.
16. Jain AK, Duin RPW, Mao J. Statistical pattern recognition: a review. *IEEE Trans Pattern Anal Mach Intell.* 2000;22:4–37.
17. Yankelevitz DF, Henschke CI. Does 2-year stability imply that pulmonary nodules are benign? *AJR Am J Roentgenol.* 1997;168:325–328.
18. Newhouse JH, Murphy RX. Tissue distribution of soluble contrast: effect of dose variation and changes with time. *AJR Am J Roentgenol.* 1981;136: 463–467.
19. Kaneko M, Eguchi K, Ohmatsu H, et al. Peripheral lung cancer: screening and detection with low-dose spiral CT versus radiography. *Radiology.* 1996;201:798–802.
20. Mori K, Tominaga K, Moriyama N, et al. Utility of low-dose helical CT as a second step after plain chest radiography for mass screening for lung cancer. *J Thorac Imaging.* 1997;12:173–180.

Int. J. Cancer: **117,** 460–468 (2005)

Identification of postoperative adjuvant chemotherapy responders in non-small cell lung cancer by novel biomarker

Takashi Hirano[1]*, Harubumi Kato[1], Masahiro Maeda[2], Yunbo Gong[1], Yanning Shou[1], Miho Nakamura[2], Junichi Maeda[1], Koichi Yashima[1], Yasufumi Kato[1], Shingo Akimoto[3], Tatsuo Ohira[1], Masahiro Tsuboi[1] and Norihiko Ikeda[1]

[1]*Department of Surgery, Tokyo Medical University, Shinjuku-ku, Tokyo, Japan*
[2]*IBL, 1091 Naka, Fujioka-City, Gunma, Japan*
[3]*MedicalProteoscope, Shinjuku-sumitomo Bldg. 7F, Nishishinjuku, Shinjuku-ku, Tokyo, Japan*

Cisplatin-based (CDDP-based) adjuvant chemotherapy of non-small cell lung cancer (NSCLC) was reported to yield 5–15% improvement in 5-year survival compared to complete resection alone. The importance of information concerning preselection of good responders has become increasingly evident. The purpose of our study is the establishment of a preselection of good responders for CDDP-based adjuvant chemotherapy. We investigated protein expressions comparing intensity between parent strains (H69 and PC14 lung cancer cultured cells) and resistant strains against CDDP using 2-dimensional polyacrylamide gel electrophoresis (2-DE). Immunohistochemically, we evaluated the relationship between protein expression associated with CDDP-resistance and the clinical effects of platinum-based postoperative adjuvant chemotherapy using 126 surgically-resected NCLC materials. We detected 2 kinds of polypeptides that changed expression levels on 2-DE gels. The analyses of the amino acid sequence showed that these polypeptides were reticulocalbin (RCN) and glutathione-*S*-transferase-π (GST-π). The 2-DE analysis showed decreased expression in RCN and overexpression in GST-π with the acquisition of CDDP-drug resistance. RCN-transfectant of H69 CDDP-resistant strain showed intermediate sensitivity between the parent strain and the CDDP-resistant strain. RCN-positive cases showed a statistically significant better disease-free survival only in the cases receiving postoperative platinum-based adjuvant chemotherapy after curative resection ($p = 0.007$). In addition, cases that were both RCN-positive and GST-π-negative showed a statistically significantly better outcome ($p = 0.0150$). In the cases without postoperative adjuvant chemotherapy no relationship between the outcome and these expressions was seen. The evaluation of RCN and GST-π might provide valuable information concerning postoperatively therapeutic strategy from the standpoint of individualized postoperative therapy.

Key words: reticulocalbin; glutathione-*S*-transferase-π; cisplatin; individual therapy; non-small cell lung cancer

Death due to lung cancer is still increasing in Japan and most Western countries, despite intensive application of various therapeutic strategies, and it is still the leading cause of cancer death in Japan. Though the opportunities of relatively early detection and treatment increase, still more than half of cases of primary lung cancer show advanced stage at the initial definitive diagnoses. Several years ago, we routinely carried out postoperative adjuvant chemotherapy using platinum (cisplatin [CDDP] or carboplatin) for patients with advanced stage non-small cell lung carcinoma (NSCLC) because distant metastasis occurred frequently after surgical treatment only. Clinically favorable outcome was not obtained, however, and the 5-year survival of Stage IIIA was approximately 25%, despite postoperative adjuvant chemotherapy. It had been believed that the efficacy of adjuvant chemotherapy in surgically resected lung cancer was controversial and that the patient's outcome was not attribute to postoperative adjuvant chemotherapy because the 1995 meta-analysis suggested that patients with complete surgical resection who received CDDP-based chemotherapy had only a 5% improvement in 5-year survival compared with those treated only by complete resection.[1]

In 2004 reports demonstrated the benefit of postoperative adjuvant chemotherapy.[2–4] The indication of postoperative chemotherapy is no longer considered controversial. We reported recently that postoperative adjuvant chemotherapy with oral UFT (DPD Inhibitory Fluoropyrimidine, Taiho Pharmaceutical Co., Ltd., Tokyo, Japan) provided better survival than surgical treatment alone in patients with Stage I adenocarcinoma of the lung.[5] We believe that the concept of postoperatively adjuvant chemotherapy that micrometastasis will be controlled does not conflict with the improvement of the prognosis in primary lung cancer. Several courses of systemic chemotherapy are usually designed. However, it is often difficult for patients who have undergone surgical resection to receive even a single course of systemic chemotherapy just after surgery. Some patients with advanced lung cancer (where surgical treatment is not indicated) sometimes respond favorably to systemic chemotherapy. It is very important, therefore, that cases that will respond well to adjuvant chemotherapy are selected.

Comprehensive analysis of human proteins (*i.e.*, proteomics) based on the establishment of human genome database has begun. Proteomics is the science by which proteins are investigated with regard to their roles as functional elements. Two-dimensional polyacrylamide gel electrophoresis (2-DE) is a strong tool in proteomics. We have applied this methodology to clinical materials of solid malignant neoplasm since 1992.[6–8] We detected some polypeptides related to drug resistance comparing 2-DE patterns of parent strains of lung cancer cultured cells with the CDDP-resistant strains. We investigated the relationship between the expression of these polypeptides and its clinically postoperative effects of patients with NSCLC.

Material and methods

Cultured cells

Lung cancer cultured cells (H69 and PC14) and their CDDP-resistant strains were kindly provided by Dr. Saijo (National Cancer Center, Tokyo, Japan).

Surgically resected NSCLC materials for 2-DE analysis

Surgically resected materials were cut in the middle and cancerous cells were collected by scraping on the surface of the tumor. After the collection of tumor cells the sample preparation for 2-DE was started as soon as possible.

2-DE polyacrylamide gel electrophoresis

In cultured cells and surgically resected materials of NSCLC we prepared samples for 2-DE using the non-enzymatic sample preparation described previously.[9] Tumor cells were fractured by repeated freezing and thawing, and the soluble fractions were lyophilized after adding DNAase-RNAase. The materials were resolubilized using a sample buffer. Isoelectric focusing (IEF) was

Grant sponsor: Japan Society for the Promotion of Science; Grant number: 10671271; Grant sponsor: Tokyo Medical University.
***Correspondence to:** Department of Surgery, Tokyo Medical University, 6-7-1 Nishishinjuku, Shinjuku-ku, Tokyo 160-0023, Japan.
Fax: +81-3-3342-6154. E-mail: thirano@tokyo-med.ac.jp
Received 8 November 2004; Accepted after revision 25 February 2005
DOI 10.1002/ijc.21172
Published online 17 May 2005 in Wiley InterScience (www.interscience.wiley.com).

TABLE I – CLINICOPATHOLOGICAL BACKGROUND OF SURGICALLY RESECTED NSCLS CASES FOR EVALUATION OF IMMUNOHISTOCHEMICAL EXPRESSION OF RETICULOCALBIN AND GST-π

	Platinum-based adjuvant chemotherapy	
	(−)	(+)
Number of cases	59 cases	67 cases
Male:Female	42:17	43:24
Age (Mean)	43–79 (65.7)	35–79 (62.6)
Histopathological type		
Adenocarcinoma	43 cases	41 cases
Squamous cell carcinoma	13 cases	21 cases
Large cell carcinoma	2 cases	2 cases
Adenosquamous cell carcinoma	1 cases	3 cases
Stage I A	23 cases	2 cases
Stage I B	17 cases	7 cases
Stage II A	3 cases	7 cases
Stage II B	6 cases	10 cases
Stage III A	8 cases	29 cases
Stage III B	2 cases	12 cases
Reduced expression of RCN	42 cases (71.2 %)	45 cases (67.2 %)
Overexpression of GST-π	29 cases (49.2 %)	33 cases (49.3 %)

used in the first dimension followed by SDS-PAGE. A sample corresponding to 30 μg of protein was applied to IEF tubes and focused for 14.5 hr at 800 V and for 1 hr at 1,000 V. After IEF, IEF gels were set on top of a linear gradient 10–13% of SDS polyacrylamide gel and electrophoresed overnight using 10 mA per gel at 10°C. After protein fixation followed by SDS-PAGE, proteins were visualized by silver staining.

Collection of polypeptides and its analysis of amino acid sequence

Polypeptides were transferred to Immobilon polyvinylidene difluoride membrane (Millipore, Bedford, MA) using the Western blotting method and visualized using Coomassie brilliant blue staining. The spots were collected from the dried Immobilon polyvinyl difluoride membrane. Collected polypeptide was applied to a gas-phase protein sequencer (HPG1005A Protein Sequencing System; Hewlett-Packard Co., Palo Alto, CA) to determine the N-terminal amino acid sequence.

Cloning of human reticulocalbin cDNA and expression in Escherichia coli *and mammalian cells*

The full-length cDNA of human reticulocalbin (RCN) was amplified from the first-strand cDNA obtained from H69 cells by using forward primer (5′-GCGGTACCGGGACGATGGCGC-GCGGTGGC-3′: hRCN-1) and reverse primer (5′-GCAAGCTTG-AGTGTCTATCAAAGCTCATC-3′: hRCN-2) synthesized and based on the published human RCN cDNA sequence. The amplified products were digested with *Kpn*I and *Hind*III, ligated into pRSET B vector (Invitrogen, Carlsbad, CA) and used to transform *E. coli* JM109 cells. RCN cDNA cloned by PCR was sequenced completely.

The full-length reticulocalbin cDNA in pRSET B vector was transferred into pcDNA3.1(+) (Invitrogen). RCN cDNA in pcDNA3.1(+) was transfected into CDDP-resistant H69 cells (H69/CDDP) by using Lipofectamine (Invitrogen). Resistant colonies against G418 were selected, cultured and cloned by limiting dilutions. The expression level of RCN protein in each stable transfectant was checked by Western blotting with anti-RCN mAb (see below). These stable transfectants were used for MTT assay against CDDP.

MTT assay of H69/CDDP cells transfected with RCN cDNA

Effect of transfected RCN cDNA on sensitivity to cisplatin in H69/CDDP cells was determined by MTT assay. Briefly, 50 μl aliquots of exponentially growing cell suspension containing 10^4 H69, H69/CDDP and H69/CDDP transfected with RCN cDNA were seeded in 96-well microtiter plates (NUNC, Rochester, NY) with 50 μl aliquots of cisplatin at various concentration (100–1.56 μM), incubated for 4 days. After incubation, 25 μl of a 3-(4,5-dimethylthiazol-2-yl)-2,5-diphenyltetrazolium bromide (NTT) (Sigma Chemical, St. Louis, MO) solution (6 mg/mL in PBS) was added to each well and the plates were incubated for 4 hr. One hundred microliters of 10% SDS solution was then added to each well and incubated at 37°C overnight. The optical density of each well was measured at 590 nm. Each experiment included triplicate wells for each cisplatin concentration and 3 independent experiments were carried out. Wells containing only medium and MTT were used as controls. We statistically estimated the difference of cellular viability at 50 μM of cisplatin in NTT assay using the Mann-Whitney *U*-test.

Production and purification of monoclonal antibodies against RCN

The synthetic peptide used for immunization was KPTVRK-ERVVRPDSELG, which corresponds to the K30 to G46 amino acid sequence of RCN. This peptide was coupled with bovine thyroglobulin and mixed with incomplete adjuvant, then injected subcutaneously (s.c.) into mice (BALB/c).

After immunization, spleen cells were collected and polyethylene glycol-mediated cell fusion between spleen cells and X63-Ag8-653 cells was induced.[10] The hybridoma cells were screened with an antigen-coated enzyme-linked immunosorbent assay (ELISA). Positive clones were cultured for production of antibodies in RPMI1640 supplemented with 10% FCS. Monoclonal antibody (mAb) was extracted from the culture medium and purified with an antigen peptide-conjugated affinity column.

Another mAb was produced against recombinant RCN protein expressed as GST fused protein in *E. coli* as follows. The C-terminal region of RCN, which corresponded to the 90 amino acid residues of RCN, was amplified from the full-length RCN cDNA obtained from H69 cells by using forward primer (5′-GCG-TCGACGGGAGCAGTTTAACGAATTCC-3′: hRCN-13) and reverse primer (5′-CTGCGGCCGCGAGTGTCTATCAAAGCT-CAT-3′: hRCN-6). The amplified products were digested with *Sal*I and *Not*I, ligated into pGEX-6P-1 vector (Amersham Bioscience, Piscataway, NJ) and used to transform *E. coli* BL21/pLys cells (RCN-C/GST). RCN-C/GST fusion protein was purified with Glutathione-Sepharose 4B (Amersham Bioscience) and used for production of mAb against C-terminal region of RCN protein as an immunogen.

The hybridoma cells were produced and screened as described above. Positive clones were cultured for production of antibodies in ASF104 media (Ajinomoto, Tokyo, Japan) as a complete medium and TIL-High-glucose (IBL) as a nutrient medium using INTEGRA CELLine culture vessel (INTEGRA Bioscience, Inc.,

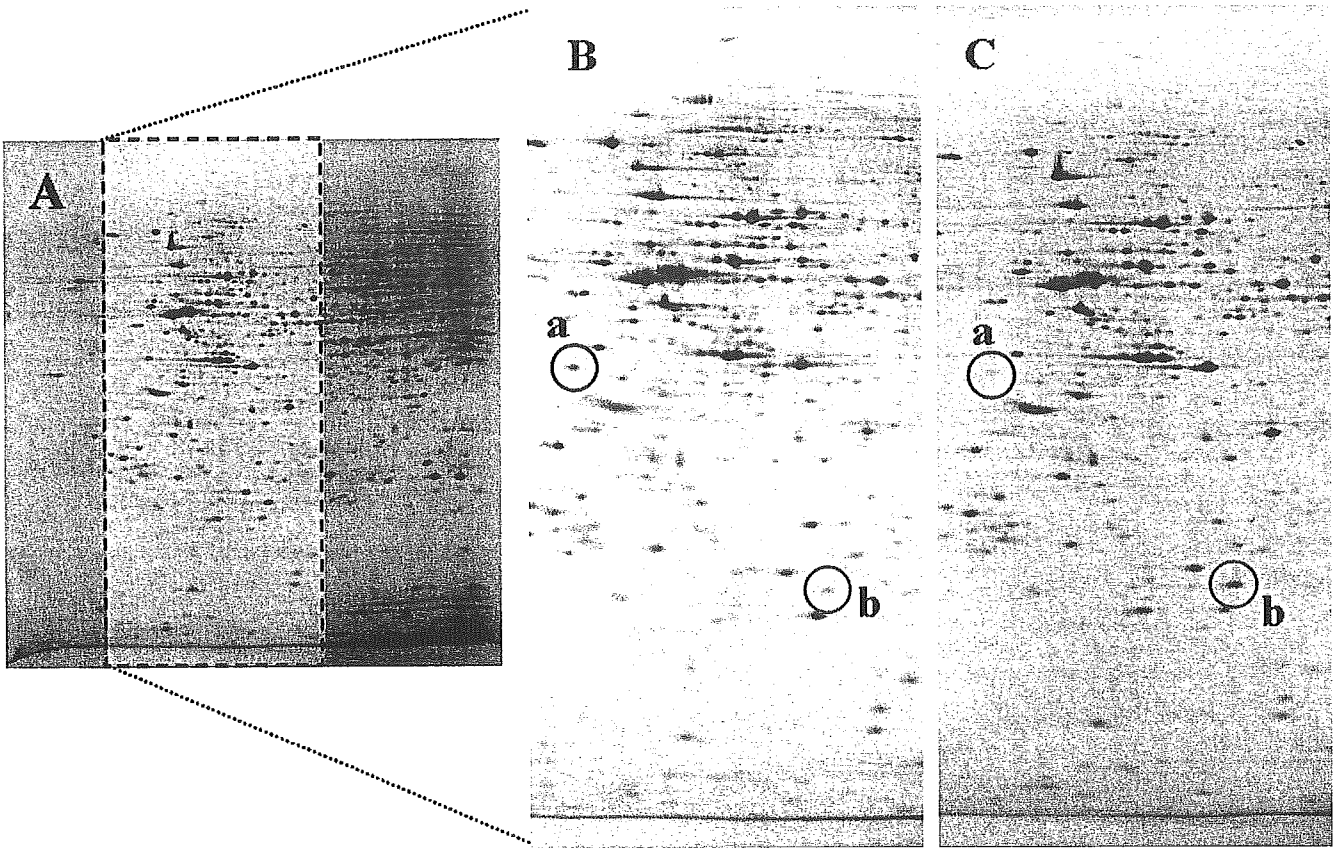

FIGURE 1 – (*a*) Overview in the 2-DE gel of H69 cultured cells. (*b*) Center area in 2-DE gel in parent strain of H69. (*c*) Center area in 2-DE gel in CDDP-resistant strain of H69. The intensity of spot a decreased remarkably in CDDP-resistant strain. The elevation of the intensity of Spot b was observed.

Chur, Switzerland) and purified with Protein A-Sepharose CL-4B affinity column (Amersham Bioscience).

Western blot and immunodetection with mAb against RCN after 2-DE

H69 cells (parent strain) were subjected to 2-DE, and proteins were transferred electrophoretically to Immobilon PVDF membrane (Millipore). The membrane was immunoblotted with anti-RCN mAbs and detection carried out with an enhanced chemiluminescence (ECL) Western detection reagents kit (Amersham Bioscience). Western blot analysis and immunodetection using anti-RCN mAbs (mAb clone 6A1 recognized the N-terminal of RCN and mAb clone M23A2 recognized the C-terminal of RCN) on H69 cells were carried out after 2-DE.

Evaluation of the expression levels of RCN and GST-π in cultured cells

H69 cells (parent strain), H69 CDDP-resistant cells and H69 CDDP-resistant strain transfected with RCN-c DNA were subjected to 1D-SDS-PAGE, and proteins were transferred and immunodetected using the same method described above. We used anti-RCN mAb (6A1) and anti-GST-π mAb for the immunodetection of each molecule.

Surgical specimens with non-small cell lung cancer and immunohistochemical staining

A total of 126 surgical specimens were obtained from patients with NSCLC resected at Tokyo Medical University Hospital between 1994–1997. Sixty-seven patients (Stage IA: 2 patients, Stage IB: 7 patients, Stage IIA: 7 patients, Stage IIB: 10 patients, Stage IIIA: 29 patients, Stage IIIB: 12 patients) were treated using platinum-based adjuvant chemotherapy (either cisplatin [CDDP] or carboplatin [CBDCA] combined with vindesine sulfate [VDS]) after complete resection. The clinicopathological background of the 126 patients with NSCLC is summarized in Table I. Four micrometer-thick tissue sections of those surgical specimens were prepared from acetone-fixed, paraffin-embedded specimens (AMeX specimens) and collected on glass slides. After deparaffinization, the specimens were stained immunohistochemically by the ABC method using mAb against RCN (clone 6A1) and GST-π (clone 353-10, DakoCytomation, Glostrup, Denmark). Meyer's hematoxylin was used for counterstaining.[11] All AMeX specimens, which had been prepared during this period, were available for the immunohistochemical investigation, and we evaluated all AMeX specimens except in the Stage IV cases (5 patients).

Statistical analysis

Statistical analysis was carried out using the StatView software system (StatView 5.0.1, SAS Institute Inc., Cary, NC). Disease-free survival curves were calculated from the day of operation by the Kaplan-Meier method and the significance of the difference in the survival rates between the patient groups was calculated by log-rank test. A p-value of <0.05 was taken to indicate a statistically significant difference.

Results

Identification of differential proteins by 2-DE

Two-dimensional polyacrylamide gel electrophoresis findings of H69 cultured cells are shown in Figure 1. The intensity of 44 kDa protein (Spot a) decreased remarkably as the CDDP resist-

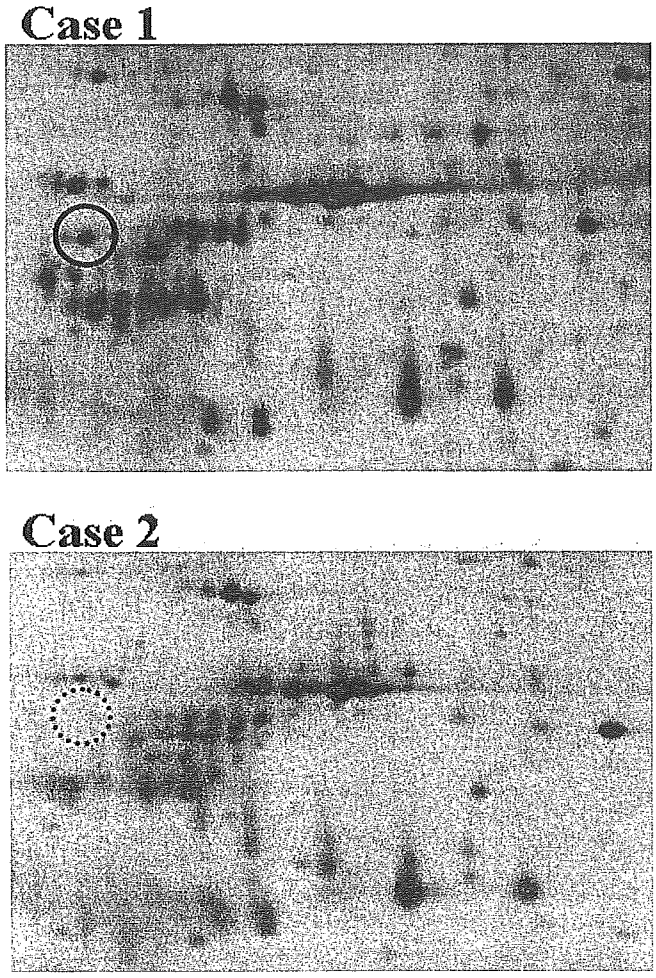

FIGURE 2 – Spot a was clearly recognized in Case 1. This case received CDDP-based adjuvant chemotherapy, and was disease-free at 5 years after complete resection. In Case 2 Spot a could not be recognized. Although Case 2 was also diagnosed as Stage IIIA as in Case 1, recurrence was recognized at 20 months after surgery.

ance was obtained. The elevation of the intensity of 23 kDa protein (Spot b) was observed. The same findings were recognized on 2-DE gels of PC14 cells. We recognized the same relationship between the intensity of these spots and responsiveness to platinum-based chemotherapy in clinical materials. Spot a was clearly detected in the cases with NSCLC that showed good prognosis with postoperatively adjuvant chemotherapy using platinum-based drugs (Fig. 2).

N-terminal amino acid sequence of Spot a and b

A 22 amino-acid N-terminal sequence of spot a was determined except for the sixth amino acid. The sequence of Spot a was KPTVR( )ERVVRPDSELGGRPPE. Also, a 20-amino acid N-terminal sequence of Spot b was determined except for amino acids 13 and 14. The sequence of Spot b was PPTYVVYFPVRG( ) ( )AALRML. Protein database examination suggested that Spot a and b was homologous with reticulocalbin (RCN) and glutathione-*S*-transferase-π (GST-π), respectively.

Microcytotoxicity assay of H69 CDDP-resistant strain transfected with RCN compared to H69 parent strain and H69 CDDP-resistant strain

We evaluated the drug sensitivity of H69 CDDP-resistant strain transfected with RCN cDNA using MTT assay comparing to parent strain and CDDP-resistant strain. RCN transfectant showed the intermediate of cell proliferation between parent strain and CDDP-resistant strain (Fig. 3). When the viability at 50 μM of CDDP was compared in our assay, there was a statistically significant difference between H69 cells (parent strain) and H69 CDDP-resistant strain transfected with vector only (Vector/H69/CDDP) ($p < 0.005$). We could not, however, detect a statistically significant difference in cellular viability between H69 cells and H69 CDDP-resistant strain transfected with RCN c DNA ($p = 0.500$). RCN transfection enhances the sensitivity of H69 CDDP-resistant strain to CDDP.

Western blot analysis using mouse mAb against RCN after 2-DE

We produced 2 kinds of mouse MAbs against N-terminal and C-terminal of RCN and designed them in mAb-6A1 and M23A2, respectively. Using each mAb against RCN, Western blot analysis of sample from H69 parent strain was carried out after 2-DE, and we confirmed that mAbs recognized Spot a (Fig. 4).

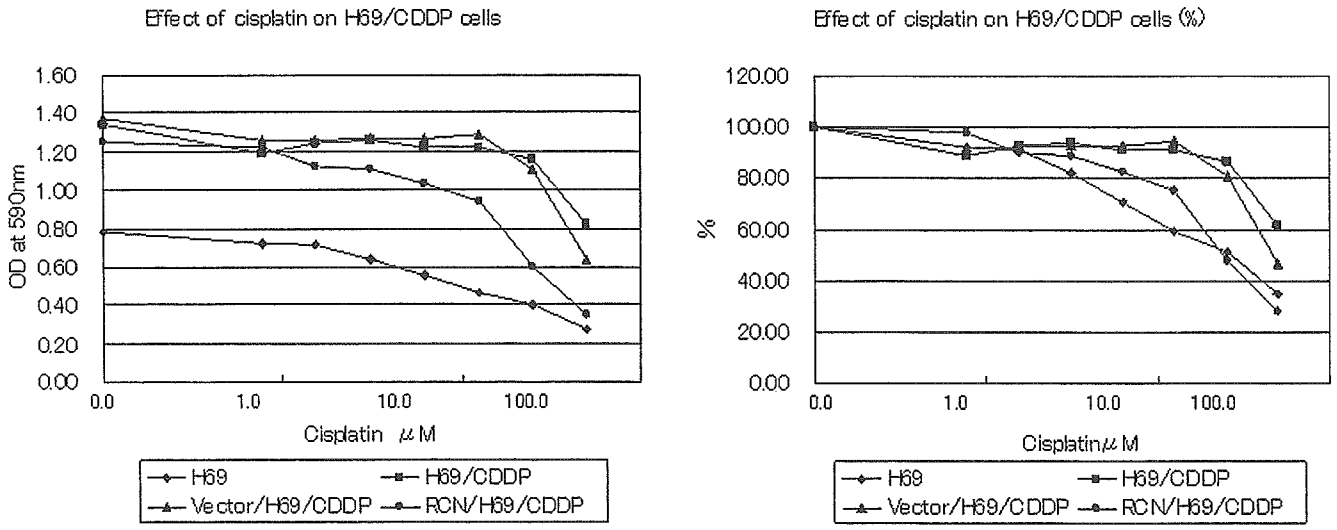

FIGURE 3 – Effects of cisplatin on H69 parent strain (H69), H69 CDDP-resistant strain (H69/CDDP) and H69 CDDP-resistant strain transfected with RCN cDNA (RCN/H69/CDDP). Exponentially growing cell suspension of H69, H69/CDDP and RCN/H69/CDDP or H69/CDDP transfected only with vector (Vector/H69/CDDP) were seeded in 96-well microtiter plates with CDDP at various concentration and incubated for 4 days. After incubation, living cells were measured by MTT assay (Material and Methods.) OD at 590 nm of each cells (*left*) and percentages (%) of each OD 590 against OD 590 without CDDP (*right*) were shown. □, H69 cell; ■, H69/CDDP cell; ▲, Vector/H69/CDDP; ●, RCN/H69/CDDP.

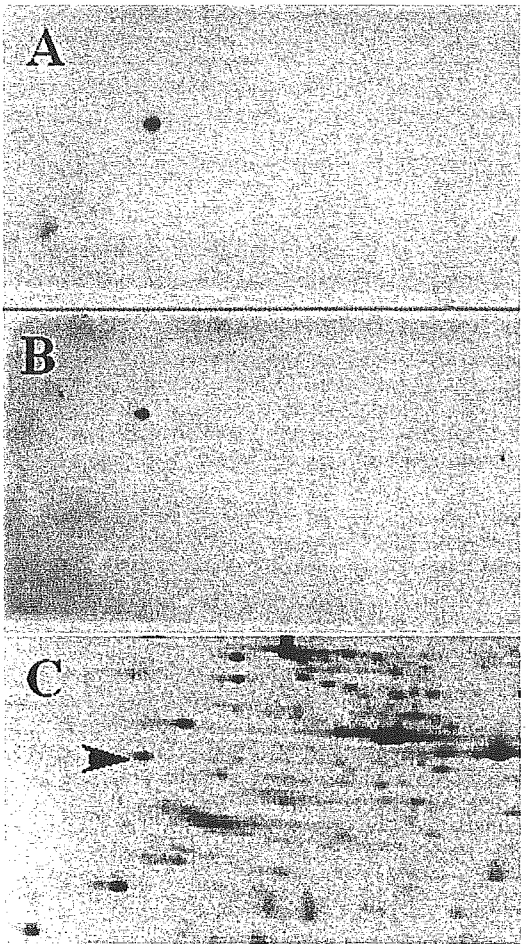

FIGURE 4 – Western blot analysis of H69 parent strain using MAbs against RCN. (*a*) mAb clone 6A1 recognized the N-terminal of RCN. (*b*) mAb clone M23A2 recognized the C-terminal of RCN. (*c*) After Western blotting, the residual proteins on the gel were visualized by silver staining. We confirmed that the spots visualized by Western blot corresponded with the RCN-spot (showing with arrowhead) on 2-DE gel.

Evaluation of the expression levels of RCN and GST-π in H69 CDDP-resistant strain transfected with RCN-c DNA using Western blot analysis

H69 CDDP-resistant strain transfected with RCN-c DNA showed high expression levels of RCN as well as GST-π (Fig. 5). In this strain GST-π expression level is similar to that of the H69 CDDP-resistant strain. The transfection of RCN-cDNA did not affect the expression levels of GST-π.

Immunohistochemical analysis of RCN and GST-π

Representative staining of RCN and GST-π is shown in Figure 6. Cytoplasmic staining was observed in RCN and GST-π. The average labeling index was 15.4% and 42.7% in reticulocalbin and GST-π, respectively. We evaluated the cases with <6% immunohistochemical reactivity of RCN as having reduced expression of RCN (negative). We also evaluated the cases with >43% immunohistochemical reactivity of GST-π as overexpression of GST-π (positive). According to these criteria, 87 of 126 cases (69.0 %) showed reduced expression (negative) of RCN and 62 cases (49.2 %) showed overexpression (positive) of GST-π. There were no relationship between pathological stage and the expression rate of either RCN or GST-π (Table II).

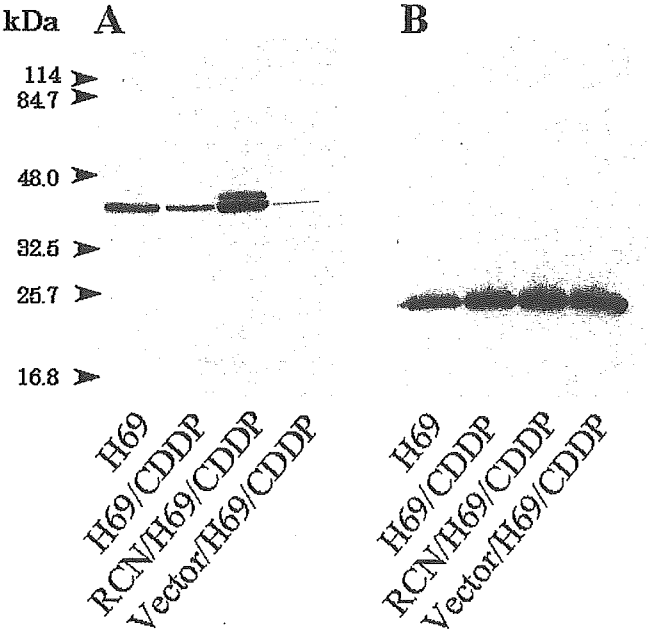

FIGURE 5 – Comparison of the expression levels of RCN and GST-π in H69 parent strain, H69/CDDP, RCN/H69/CDDP and Vector/H69/CDDP. (*a*) Western blot analysis using mAb against RCN (clone 6A1). (*b*) Western blot analysis using mAb against GST-π. H69, H69 parent strain; H69/CDDP, H69 CDDP resistant strain; RCN/H69/CDDP, H69 CDDP transfected RCN; Vector/H69/CDDP, H69/CDDP transfected with vector. RCN/H69/CDDP cells exhibited higher expression of RCN than H69 CDDP. We could not recognize a remarkable change of expression level of GST-π compared to H69/CDDP.

Disease-free survival and the expression of RCN or GST-π

RCN. Non-relapse mortality curves of cases without adjuvant chemotherapy are shown in Figure 7*b*. We did not detect statistically significant differences between cases with and without the expression of RCN. In cases with platinum-based adjuvant chemotherapy, however, there was a statistically significant difference between cases with and without RCN expression ($p = 0.007$) (Fig. 7*a*).

GST-π. The non-relapse mortality curves of cases with/without adjuvant chemotherapy are shown in Figure 8. There was a statistically significant difference between cases with and without expression of GST-π only in cases with platinum-based adjuvant chemotherapy ($p = 0.0219$).

Disease-free survival and co-evaluation of RCN and GST-π

When we evaluated pathological Stage IIA–IIIB cases with postoperative adjuvant chemotherapy, the non-relapse mortality rate in the cases with positive RCN expression and negative expression of GST-π was 66.0%. It was <20% in the cases with the other combinations of RCN and GST-π expressions. There were statistically significant differences recognized between cases with positive expression of RCN and negative expression of GST-π and cases with other combination of these proteins ($p = 0.0150$) (Fig. 9).

Discussion

Distant metastases occur frequently in patients with advanced stage-NSCLC who undergo only surgery, perhaps because micrometastasis exists at the time of surgical treatment. We believe that the concept of postoperatively adjuvant chemotherapy for control of micro-metastasis does not conflict with the improvement of the prognosis in NCLC. The efficacy of postoperative adjuvant chemotherapy in completely resected NCLC, however, used to be controversial.[12,13] According to a previous meta-analysis, postoperative adjuvant chemotherapy using platinum-based

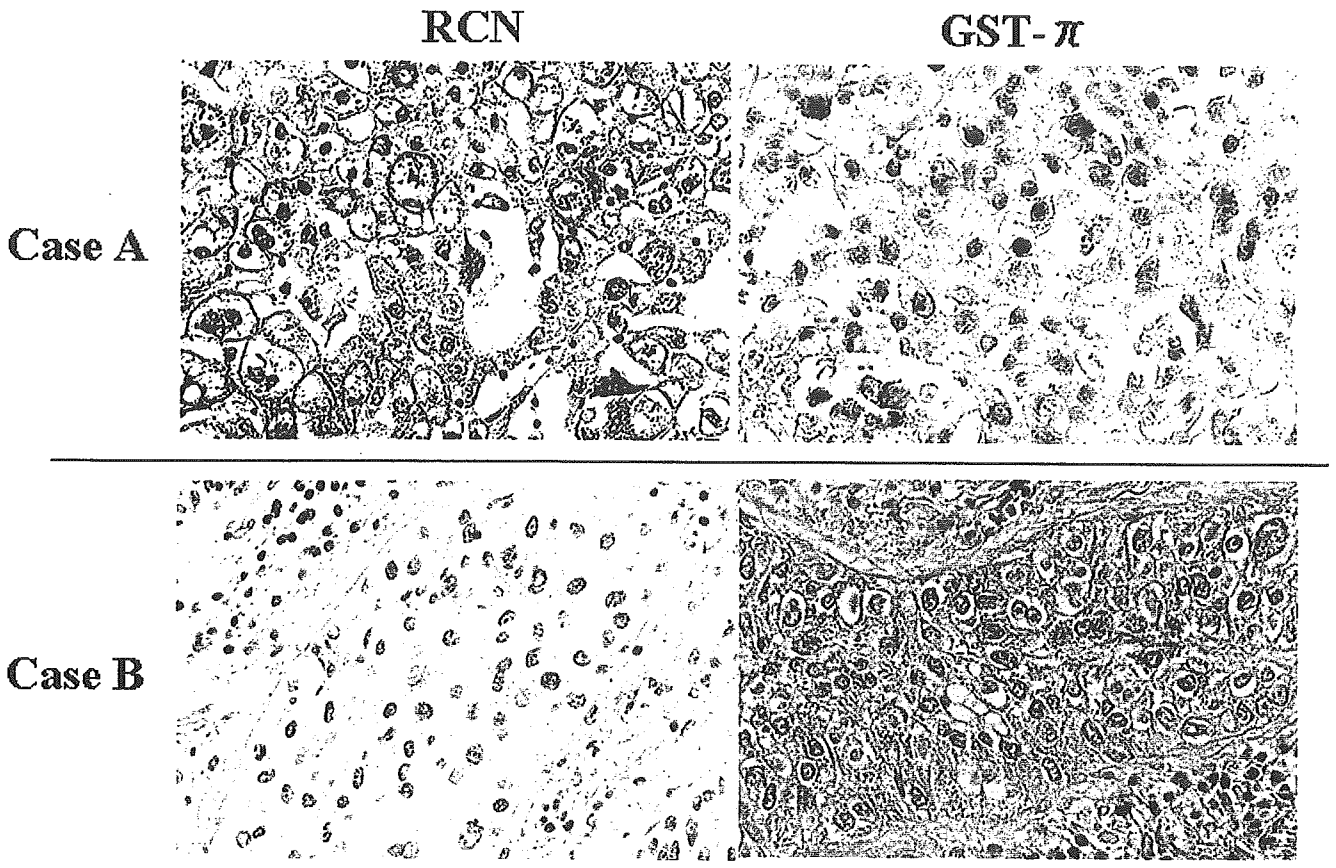

FIGURE 6 – Immunohistochemical reactivity of representative cases using anti-RCN mAb (clone 6A1) and anti-GST-π mAb (clone 353-10, DakoCytomation). Case A showed positive cytoplasmic staining of RCN and negative immunohistochemical reactivity of GST-π. Case B showed negative immunohistochemical reactivity of RCN and positive cytoplasmic staining of GST-π.

agents is generally not effective for survival improvement of patients with NSCLC. Several adjuvant chemotherapy trials in the late 1990s after an individual data-based meta-analysis suggested a 5% increase in survival at 5 years.[1] The results of 2 randomized trials to assess the benefit of adjuvant chemotherapy in patients with early-stage NSCLC were reported at the 40th Annual Meeting of the American Society of Clinical Oncology.[3,4] Furthermore, a recent large scale randomized clinical trial launched just after the publication of the meta-analysis concluded that patients assigned to CDDP-based postoperative adjuvant chemotherapy had a statistically significantly higher survival rate than those assigned to postoperative observation (44.5% *vs.* 40.4% at 5 years; $p < 0.03$).[2] Even though a statistically significant difference was found in this study, 5-year-survival rate benefit was approximately 5–15%. It may seem that leading lung cancer experts have reached a consensus concerning postoperatively adjuvant chemotherapy.

We propose that rather than focusing only on improving chemotherapy regimens, we should also make efforts to identify patients who will show good response for already established chemotherapy regimens. We believe that this proposal is justified based only on the results of evidence-based medicine. We attempted to detect novel biomarkers for selection of well-responders using proteomic analysis.

Two-dimensional polyacrylamide gel electrophoresis enables simultaneous evaluation of a large number of polypeptides.[14] Most cellular functions are controlled by protein–protein interaction and we believe that proteomic analysis is the best strategy for understanding various kinds of clinical phenomenon. Our study simultaneously detected 2 kinds polypeptides related to drug resistance by comparing 2-DE patterns of parent strains of lung cancer cultured cells and their CDDP-resistant strains. When strains obtained CDDP-drug resistance, one polypeptide showed reduced expression, whereas the other one showed overexpression. N-terminal of amino-acid sequence analysis showed that the former was RCN and that the latter was GST-π.

TABLE II – RELATIONSHIP BETWEEN PATHOLOGICAL STAGE AND IMMUNOHISTOCHEMICAL REACTIVITY OF RCN AND GST-π

Stage	Reduced expression of RCN	Overexpression of GST-π
I A	19/25 (76.0%)	10/25 (40.0%)
I B	15/24 (62.5%)	12/24 (50.0%)
II A	6/10 (60.0%)	5/10 (50.0%)
II B	12/16 (75.0%)	5/16 (31.3%)
III A	28/37 (75.7%)	22/37 (59.5%)
III B	7/14 (50.0%)	8/14 (57.1%)
Total	87/126 (69.0%)	62/126 (49.2%)

GST-π is an enzyme involved with cellular detoxification of many xenobiotic substances through conjugation to glutathione and degrading oxygen free radicals.[15–17] It is already well-known that GST-π overexpression is associated with increased resistance to platinum-based chemotherapy and poor outcome in NSCLC.[18,19]

RCN is an endoplasmic reticulum-resident Ca^{2+}-binding protein with 6 repeats of a domain containing the EF-hand motif. RCN is reported to be a luminal protein with molecular weight 44 kDa.[20–23] The RCN molecule is probably necessary for normal behavior of cells because homozygous deletion in mice of RCN could contribute to the lethality.[24] Although the detailed physiological functions of RCN are still unknown, a few investigators reported that RCN expressed in malignant neoplasms. Yu et al.[25] reported overexpression of RCN in hep-

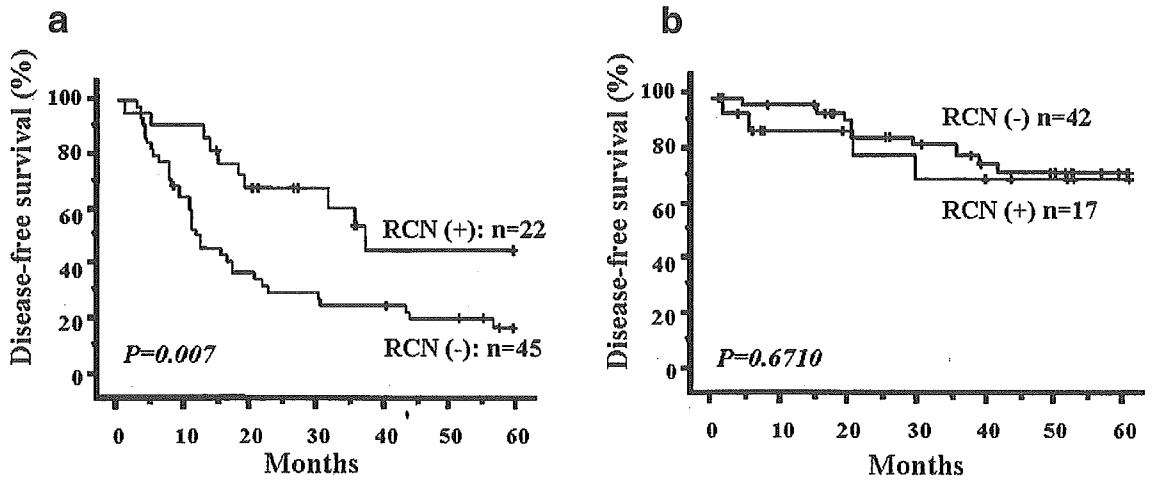

FIGURE 7 – Kaplan-Meier curves for disease-free survival from complete resection in pathological Stage IA–IIIB NSCLC cases with postoperative adjuvant chemotherapy using platinum (*a*) or without any adjuvant chemotherapy (*b*). When we evaluated cases with platinum-based adjuvant chemotherapy, RCN-positive cases showed statistically significant higher survival than RCN-negative cases ($p = 0.007$). In cases without adjuvant chemotherapy, there was no statistically significant difference in disease-free survival between 2 groups with or without RCN expression.

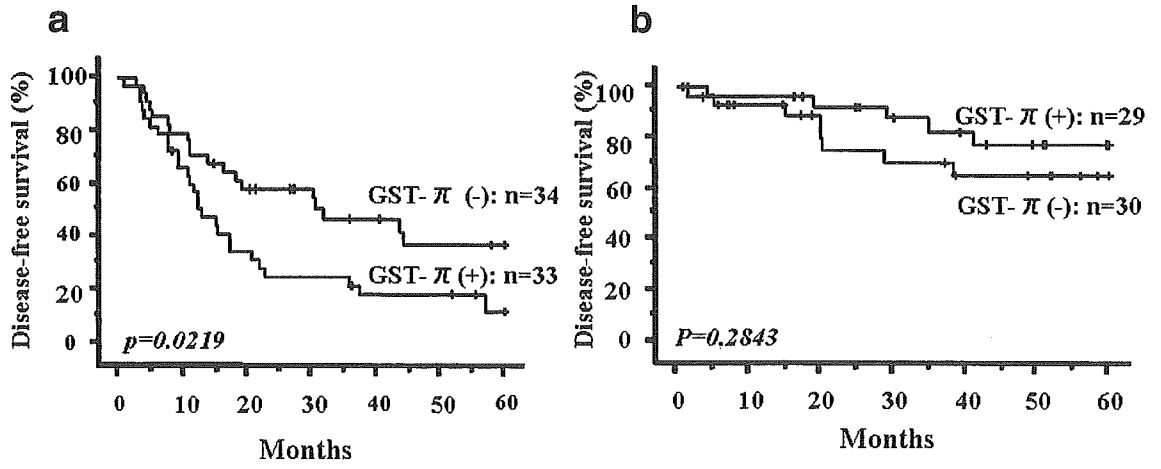

FIGURE 8 – Kaplan-Meier curves for disease-free survival from complete resection in pathological Stage IA–IIIB NSCLC cases with postoperative adjuvant chemotherapy using platinum (*a*) or without any postoperative adjuvant chemotherapy (*b*). When we evaluated cases with platinum-based adjuvant chemotherapy, GST-π-negative cases showed statistically significant higher survival than GST-π-positive cases ($p = 0.0219$). In cases without adjuvant chemotherapy, there was no statistically significant difference in disease-free survival between 2 groups with or without GST-π expression.

atoma compared to normal liver cells. It was also reported that RCN was expressed in highly invasive breast cancer cell lines but not in poorly invasive lines in matrigel invasion assays.[26] Liu *et al.*[26] suggested the high expression of RCN correlated with a low expression of the Ca^{2+}-dependent cell adhesion molecule cadherin in these cell lines. There are no reports, however, concerning the relationship between the expression of RCN and drug-resistance in malignant neoplasms.

The 2-DE findings of lung cancer cultured cells suggested that a decreased expression level of RCN was deeply related with drug-resistance to CDDP. Furthermore, as CDDP-resistant strain transfected RCN c-DNA, the transfectant showed an intermediate sensitivity to CDDP between the sensitivity of the parent strain and that of the CDDP-resistant strain, indicating that RCN c-DNA transfection enhanced the sensitivity to CDDP. We evaluated the outcome of the patients that received postoperative adjuvant chemotherapy using platinum based agents. We recognized a statistically significant association between positive RCN expression and good outcome. No such association was observed in cases without postoperative adjuvant chemotherapy. Furthermore, we showed no relationship between pathological stages and the expression rate of RCN in Table II. Therefore, we concluded that RCN is an important molecule related to CDDP-drug resistance.

We attempted to evaluate the relationship between the co-expressions of RCN and GST-π and disease-free survival of more advanced NSCLC cases (pathological Stage IIA–IIIB) because remarkable changes of these 2 kinds of polypeptides were observed simultaneously on 2-DE gels. These changes were also commonly shown and reproducibly observed in 2 kinds of lung cancer cell lines. Disease-free survival probability showed that only the group with positive RCN expression and negative expression of GST-π was associated significantly with a good outcome. The 5-year disease free survival rate of the group was 66.0%. This favorable survival rate showing positive RCN and negative GST-π corresponds to that of Stage I-NSCLC. Positive RCN and GST-π-negative expression cases should be considered as good indications of platinum-based postoperative adjuvant chemotherapy.

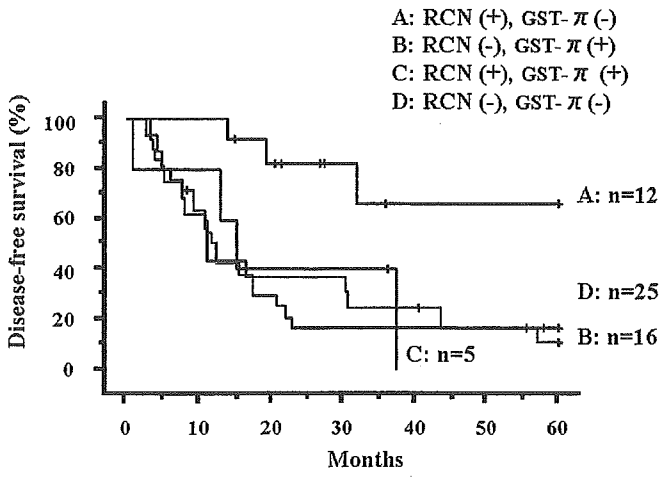

FIGURE 9 – Kaplan-Meier curves for disease-free survival from complete resection in pathological Stage IIA–IIIB NSCLC cases with postoperative adjuvant chemotherapy using platinum. (*a*) Cases with positive RCN-expression and negative GST-π expression (non-relapse mortality rate at 5-years = 66.0%). (*b*) Cases with negative RCN-expression and positive GST-π expression (non-relapse mortality rate at 5-years = 11.3%). (*c*) Cases with positive expression of both RCN and GST-π (non-relapse mortality rate at 5-years = 0 %). (*d*) Cases with negative expression of both RCN and GST-π (non-relapse mortality rate at 5-years = 16.7 %). Group A showed statistically significant higher survival than the other groups (A–B, $p = 0.0007$; A–C, $p = 0.0388$; A–D, $p = 0.0065$).

Therefore, we concluded that this result provided an important information concerning pre-selection of patients who would benefit from postoperatively adjuvant chemotherapy using platinum.

Until the results of 2 randomized trials to assess the benefit of adjuvant chemotherapy in patients with early-stage NSCLC were reported at the 40th Annual Meeting of the American Society of Clinical Oncology,[3,4]) we had no evidence concerning the efficacy of adjuvant chemotherapy. We believed that severe adjuvant chemotherapy led to poor prognosis. In our study, we have enough Stage I NSCLC patients to evaluate the relationship between efficacy and the expression of these molecules. We could not avoid excluding Stage I NSCLC cases in the evaluation of the relationship between the co-expressions of RCN and GST-π and disease-free survival.

Individual therapy for lung cancer patients is attracting attention. Therapeutic strategies should be different for each patient. We do not know, however, that individual therapy for lung cancer is realized routinely in clinical. For more than 20 years it has been believed that platinum based-chemotherapy is one of the most important therapeutic strategies for lung cancer patients who lack indications of surgical treatment, and complete response has been shown in some patients untreated previously. At the same time, we believe that platinum-based chemotherapy is one of the most useful strategies to control systemic micro-metastasis after complete resection. Co-evaluation of RCN and GST-π might provide valuable information concerning the selection of postoperatively platinum-based adjuvant chemotherapy and we believe that this kind of proteomic evaluation would be realizing postoperative individual therapy based upon medical evidences.

We emphasize that downregulation of RCN was independent of GST-π expression and our study is the first article concerning the relationship between the efficacy of platinum-based adjuvant chemotherapy and co-expression of RCN and GST-π.

Acknowledgements

We would like to thank Professor J.P. Barron of the International Medical Communications Center of Tokyo Medical University for reviewing this manuscript. We are also grateful to Dr. Saijo, National Cancer Center, for the gift of CDDP-resistant strains of lung cancer cultured cells.

References

1. Non-Small Cell Lung Cancer Collaborative Group. Chemotherapy in non-small cell lung cancer: a meta-analysis using updated data on individual patients from 52 randomized clinical trials. Br Med J 1995; 311:899–909.
2. Arriagada R, Bergman B, Dunant A, Le Chevalier T, Pignon JP, Vansteenkiste J. (International Adjuvant Lung Cancer Trial Collaborative Group) Cisplatin-based adjuvant chemotherapy in patients with completely resected non-small-cell lung cancer. N Engl J Med 2004; 350:351–60.
3. Winton TL, Livingston R, Johnson D, Rigas J, Cormier Y, Butts C, Ding K, Seymour L, Magoski N, Shepherd F. A prospective randomized trial of adjuvant vinorelbine (VIN) and cisplatin (CIS) in completely resected stage IB and II non small cell lung cancer (NSCLC) Intergroup JBR. 10. Proc Am Soc Clin Oncol 2004;23:621.
4. Strauss GM, Herndon J, Maddaus MA, Johnstone DW, Johnson EA, Watson DM, Sugarbaker DJ, Schilsky RL, Green MR. Randomized clinical trial of adjuvant chemotherapy with paclitaxel and carboplatin following resection in stage IB non-small cell lung cancer (NSCLC): report of Cancer and Leukemia Group B (CALGB) Protocol 9633. Proc Am Soc Clin Oncol 2004;23:621.
5. Kato H, Ichinose Y, Ohta M, Hata E, Tsubota N, Tada H, Watanabe Y, Wada H, Tsuboi M, Hamajima N, Ohta M, for the Japan Lung Cancer Research Group on Postsurgical Adjuvant Chemotherapy. A randomized trial of adjuvant chemotherapy with Uracil-Tegafur for adenocarcinoma of the lung. N Engl J Med 2004;350:1713–21.
6. Hirano T, Franzen B, Uryu K, Okuzawa K, Alaiya AA, Vanky F, Rodrigues L, Ebihara Y, Kato H, Auer G. Detection of polypeptides associated with the histopathological differentiation of primary lung carcinoma. Br J Cancer 1995;72:840–8.
7. Franzen B, Auer G, Alaiya AA, Eriksson E, Uryu K, Hirano T, Okuzawa K, Kato H, Linder S. Assessment of homogeneity in polypeptide expression in breast carcinomas shows widely variable expression in highly malignant tumors. Int J Cancer 1996;69:408–14.
8. Hirano T, Auer G, Maeda M, Hagiwara Y, Okada S, Ohira T, Okuzawa K, Fujioka K, Franzen B, Hibi N, Seito T, Ebihara Y, Kato H. Human tissue distribution of TA02, which is homologous with a new type of aspartic Proteinase, napsin A. Jpn J Cancer Res 2000;91: 1015–21.
9. Franzen B, Linder S, Okuzawa K, Kato H, Auer G. Non-enzymatic extraction of cells from clinical tumor material for analysis of gene expression by two-dimensional polyacrylamide gel electrophoresis. Electrophoresis 1993;14:1045–53.
10. Banno S, Yoshikawa K, Nakamura S, Yamamoto K, Seito T, Nitta M, Takahashi T, Ueda R, Sero M. Monoclonal antibody against PRAD1/cyclin D1 stains nuclei of tumor cells with translocation or amplification at BCL-1 locus. Jpn J Cancer Res 1994;85:918–26.
11. Shou Y, Hirano T, Gong Y, Kato Y, Yoshida K, Ohira T, Ikeda N, Konaka C, Ebihara Y, Zhao F, Kato H. Influence of angiogenetic factors and matrix metalloproteinases upon tumour progression in non-small-cell lung cancer. Br J Cancer 2001;85:1706–12.
12. Pisters KM. Stage I/II non-small cell lung cancer: is there a role for combined-modality therapy? American Society of Clinical Oncology (2002 educational book), ASCO Publications, Alexandria, 2002:465–70.
13. Scagliotti GV, Fossati R, Torri V, Giaccone G, Silvano G, Martelli M, Clerici M, Cognetti F, Tonato M. Randomized study of adjuvant chemotherapy for completely resected stage I, II, or IIIA non-small-cell lung cancer. J Natl Cancer Inst 2003;95:1453–61.
14. Okuzawa K, Franzen B, Lindholm J, Hirano T, Bergman T, Ebihara Y, Kato H, Auer G. Characterization of gene expression in clinical lung cancer material by two-dimensional polyacrylamide gel electrophoresis. Electrophoresis 1994;15:382–90.
15. Mannervik B. The enzymes of glutathione metabolism: an overview. Biochem Soc Trans 1987;15:717–8.
16. Tew KD. Glutathione-associated enzymes in anticancer drug resistance. Cancer Res 1994;54:4313–20.
17. Goto S, Kamada K, Soh Y, Ihara Y, Kondo T. Significance of nuclear glutathione S-transferase pi in resistance to anti-cancer drugs. Jpn J Cancer Res 2002;93:1047–56.
18. Arai T, Yasuda Y, Takaya T, Hayakawa K, Toshima S, Shibuya C, Kashiki Y, Yoshimi N, Shibayama M. Immunohistochemical expression